Rita de Sousa Gorgulho

Bachelor in Biology

Usefulness of zebrafish model to assess glomerular and tubular alterations induced by tenofovir

Dissertação para obtenção do Grau de Mestre em
Genética Molecular e Biomedicina

Orientadora: Judit Morello, Professora Auxiliar, NOVA Medical School, UNL

Co-orientadora: Sofia A. Pereira, Professora Auxiliar, NOVA Medical School, UNL

Júri:

Presidente: Doutora Margarida Casal Ribeiro Castro Caldas Braga

Vogais: Doutora Judit Morello Bullón

Doutor Miguel Alberto Fernandes Machado e Santos

FACULDADE DE CIÊNCIAS E TECNOLOGIA
UNIVERSIDADE NOVA DE LISBOA

Setembro de 2015

Usefulness of zebrafish model to assess glomerular and tubular alterations induced by tenofovir

The current work was funded by:

Fundação Calouste Gulbenkian. Gulbenkian Professorship (2012). Project 121986.

The results discussed in this thesis originated:

Publications in international scientific journals:

Gorgulho, R. S., Lopes, S., Correia, A. C., Tranfield, E. M., Monteiro, E. C., Pereira, S. A., Morello, J. 2015. Usefulness of zebrafish model to assess glomerular and tubular alterations induced by nephrotoxic drugs. Toxic Letters. Volume 238 (2S). ISSN 0378-4274.

Posters in international meetings:

Gorgulho, R. S., Lopes, S., Correia, A. C., Tranfield, E. M., Monteiro, E. C., Pereira, S. A., Morello, J. Usefulness of zebrafish model to assess glomerular and tubular alterations induced by nephrotoxic drugs. Poster for the 51st Congress of the European Societies of Toxicology (Eurotox). Porto, Portugal. 2015.

Oral communications in national meetings:

Gorgulho, R. S., Lopes, S., E. M., Monteiro, E. C., Pereira, S. A., Morello, J. Monitoring glomerular function in zebrafish larvae (*Danio rerio*) exposed to nephrotoxic drugs. XLV SPF (Sociedade Protuguesa de Farmacologia) Meeting. NOVA Medical School. Lisbon, Portugal. 5 – 6 February 2015.

Gorgulho, R. S., Pereira, S. A., Morello, J. Evaluation of Tenofovir-induced mitochondrial toxicity in the zebrafish model. Jornadas Intercalares das Dissertações Anuais dos Mestrados. Faculdade de Ciências e Tecnologia – Universidade Nova de Lisboa. Lisboa, Portugal. 2015.

Awards:

Entry Bursary for the 51st Congress of the European Societies of Toxicology (Eurotox). Bridging Sciences for Safety. Porto, Portugal. 13 – 16 September 2015.

In memory of Ruca,

You will be forever missed

Acknowledgements

A realização desta tese teria sido impossível sem a ajuda de inúmeras pessoas. Por isso irei aproveitar este espaço para reconhecer a preciosa ajuda que me prestaram.

Em primeiro lugar quero agradecer à minha orientadora, a Judit Morello, não só pela oportunidade que me deu para a realização deste trabalho (que adorei!) mas principalmente pela incansável ajuda que me prestou ao longo do ano e por tudo o que me ensinou. Também gostaria de agradecer à minha co-orientadora, Sofia Azeredo Pereira, por toda a ajuda que me deu e também pela preciosa oportunidade.

Também quero agradecer ao grupo do laboratório que me acolheu no IGC. Nunca tinha trabalhado num ambiente tão acolhedor e dinâmico. Ajudaram-me sempre no que precisei e sem dúvida que me ensinaram imensas coisas novas. Por isso, deixo o meu especial agradecimento à Susana Lopes, à Bárbara e à Raquel (adorei as nossas conversas sobre os livros!), à Mónica, à Petra, ao Pedro, à Diana e à Hanna.

Também não podia deixar de agradecer à Catarina e à Erin, do departamento de microscopia eletrónica, por toda a ajuda com o TEM e por me terem ensinado tanto.

Agradeço também ao grupo do laboratório de farmacologia, que, apesar de a minha estadia ter sido curta nesse lado, acolheu-me de braços abertos. Deixo um especial agradecimento à Clara por toda a ajuda na submissão do poster e pela excelente companhia no Porto.

Claro que também não podia deixar de agradecer à minha família e amigos. Obrigada pelo incansável suporte e carinho. Agradeço especialmente à minha mãe, por me ir lembrando de comer qualquer coisa, e ao meu pai que literalmente contribuiu na escrita desta tese. E suponho que também tenho de agradecer à minha irmã por…bem…eu hei de me lembrar de qualquer coisa (*edit*: por ter me ter dado a conhecer LoL e animes, e por ser a minha fonte de informação de eventos e coisas interessantes da internet – quando se lembra de mos contar).

Por último, agradeço ainda aos meus gatos (2ª vez que me fazem companhia à noite na escrita de um trabalho!) e à minha cadela por ser tão querida.

E deixo ainda o meu mais profundo e sincero agradecimento ao Ruca, o cão mais meigo que conheci, pelos 13 anos que passaste connosco. Infelizmente já não estás aqui para te poder agradecer pessoalmente, mas sabes que nunca te vamos esquecer.

Bjnhos**

Abstract

Tenofovir (TFV) is one of the most used antiretroviral drugs. However, it is associated with tubular damage with mitochondria as a possible target. Tubulopathy precedes glomerular dysfunction, thus classic markers of renal function like the glomerular filtration rate (GFR) do not detect early TFV damage. Prediction and management of drug induced renal injury (DIRI) rely on the mechanisms of the drug insult and in optimal animal models to explore it. Zebrafish (*Danio rerio*) offers unique advantages for assessing DIRI, since the pronephros is structurally very similar to its human counterpart and is fully developed at 3.5 days postfertilization.

The main aim of the present work was to evaluate the effects of TFV, as well as its pro-drug, tenofovir disoproxil fumarate (TDF), on the GFR and in mitochondria morphology in tubular cells of zebrafish larvae.

Lethality curves were performed to understand the relationship between drug concentration and lethality. LC_{10} was selected to explore the renal function using the FITC-inulin assay and to analyze the mitochondrial toxicity by electron microscopy on larvae exposed to TDF, TFV, paracetamol and gentamicin (positive controls) or water (negative control).

Lethality curves showed that gentamicin was the most lethal drug, followed by TDF, TFV and paracetamol. Gentamicin and paracetamol decreased the GFR, but no differences were found for either TDF or TFV, when compared to controls (%FITC Control = 33±8; %FITC TDF = 35±10; %FITC TFV = 30±10; %FITC Gentamicin = 46±17; %FITC Paracetamol = 83±14). Tubular mitochondria from treated larvae were notably different from non-treated larvae, showing swelling, irregular shapes, decreased mitochondria network, cristae disruption and loss of matrix granules.

These results are in agreement with the effects of these drugs in humans and thus, demonstrate that zebrafish larvae can be a good model to assess the functional and structural damage associated with DIRI.

Keywords

Zebrafish, tenofovir, drug induced renal injury, glomerular function, transmission electron microscopy.

Resumo

Tenofovir (TFV) é um dos fármacos antirretrovirais mais utilizados. No entanto, está associado a danos tubulares, sendo a mitocôndria um dos possíveis alvos. Tubulopatia precede a disfunção glomerular, o que indica que marcadores clássicos da função renal, como a taxa de filtração glomerular (TFG) não conseguem detetar danos prematuros induzidos por TFV. Previsão e gestão de danos renais induzidos por fármacos (DRIF) dependem dos mecanismos da toxicidade causada pelo fármaco e em animais modelos para o explorarem. O peixe-zebra (*Danio rerio*) oferece vantagens únicas no estudo de DRIF, uma vez que o prónefro é estruturalmente muito semelhante ao seu homólogo humano e encontra-se completamente desenvolvido aos 3.5 dias pós-fertilização.

O objetivo principal desta tese é avaliar os efeitos do TFV, bem como do pró-fármaco tenofovir disoproxil fumarato (TDF), na TGF e na morfologia das mitocôndrias de células tubulares de larvas de peixe-zebra.

Foram calculadas curvas de letalidade com o objetivo de encontrar a relação entre as concentrações do fármaco e a letalidade causada. LC_{10} foi escolhida para analisar a função renal, através do ensaio com FITC-inulina, e para analisar toxicidade mitocondrial, por microscopia eletrónica, em larvas expostas a TDF, TFV, paracetamol e gentamicina (controlos positivos) ou água (controlo negativo).

As curvas de letalidade mostraram que a gentamicina foi o fármaco mais potente, seguido pelo TDF, TFV e paracetamol. A gentamicina e o paracetamol diminuíram a TFG, no entanto não foram observadas diferenças entre TDF e TFV, quando comparados com o controlo (%FITC Controlo = 33±8; %FITC TDF = 35±10; %FITC TFV = 30±10; %FITC Gentamicina = 46±17; %FITC Paracetamol = 83±14). Mitocôndrias tubulares de larvas tratadas eram bastante diferentes de larvas não-tratadas, apresentando inchaço, formas irregulares, diminuta rede mitocondrial, disrupção das cristas e perda de grânulos da matriz.

Estes resultados estão de acordo com os efeitos observados em humanos, o que demonstra que as larvas do peixe-zebra podem ser um bom modelo para analisar danos funcionais e estruturais associados a DRIF.

Palavras-chave

Peixe-zebra, tenofovir, danos renais induzidos por fármacos, função glomerular, microscopia eletrónica de transmissão

Contents

Acronyms

AIDS	Acquired Immunodeficiency Syndrome
AKI	Acute Kidney Injury
ART	Antiretroviral Therapy
ARV	Antiretroviral
AZT	Azidothymidine
CCV	Common Cardinal Vein
CDC	Centers for Disease Control
cdh17	*cadherin-17*
CKD	Chronic Kidney Disease
DIRI	Drug Induced Renal Injury
dpf	Days post fertilization
DRIF	Danos Renais Induzidos por Fármacos
EM	Embryo media
FACS	Fluorescence-Activated Cell Sorting
FDA	U.S. Food and Drug Administration
FITC	Fluorescein Isothiocyanate
GFR	Glomerular Filtration Rate
HAART	Highly Active Antiretroviral Therapy
HIV	Human Immunodeficiency Virus
HIVAN	HIV-Associated Nephrotoxicity
HIVICK	HIV Immune-Complex Kidney Disease
hpf	Hours post fertilization

IGC	Gulbenkian Institute of Science
INSTI	Integrase Strand Transfer Inhibitor
LC_{10}	Lethal Concentration for 10% of the population
LC_{50}	Lethal Concentration for 50% of the population
MDGs	UN Millennium Development Goals
mtDNA	Mitochondrial DNA
NNRTI	Non-Nucleoside Reverse-Transcriptase Inhibitor
NRTIs	Nucleoside Reverse-Transcriptase Inhibitors
OAT	Organic Anion Transporters
OIs	Opportunistic Infections
PCNA	Proliferating Cell Nuclear Antigen
PCP	*Pneumocystis jiroveci* pneumonia
PIs	Proteinase Inibitors
RNS	Reactive Nitrogen Species
ROS	Reactive Oxygen Species
TD	Tenofovir Diphosphate
TDF	Tenofovir Disoproxil Fumarate
TEM	Transmission Electron Microscopy
TFV	Tenofovir Monophosphate
TUNEL	Terminal deoxynucleotidyl transferase dUTP nick end labeling
UN	United Nations
UNAIDS	Joint United Nations Program on HIV/AIDS
UNGASS	United General Assembly Special Session on HIV/AIDS
WHO	World Health Organization

Wt1b	*Wilms tumor suppressor*

List of figures

List of tables

Introduction

1. HIV/AIDS

a. Brief history of HIV/AIDS – How the epidemic started

It is believed that HIV (Human Immunodeficiency Virus), the virus responsible of AIDS (Acquired Immunodeficiency Syndrome), was probably transferred to humans from primates in Africa between 1884 and 1924. There are several theories regarding it, one of them being that the virus was transmitted either from blood contact, by wounds of hunters that entered in contact with infected primate blood, or via sexual contact. But the epidemic probably started its spread due to vaccination of thousands of people with same needle, in the area where HIV transmission happened (http://www.avert.org/).

Up until 1981, there were no reports associated to AIDS, as the disease was yet unknown and disguised as opportunistic infections (OIs) that were acquired by a deficiency of the immune system (http://www.avert.org/). Several earlier cases were later linked to it, thought. As Jonathan Mann *apud* http://www.avert.org/ said, "*The dominant feature of this first period was silence, for the human immunodeficiency virus was unknown and transmission was not accompanied by signs or symptoms salient enough to be noticed*.". During this period of silence, approximately 100,000-300,000 persons were estimated to have been infected unknowingly and unwarily (http://www.avert.org/).

It was only in June 1981 that the world first became aware of a rising epidemic (http://www.avert.org/; WHO, 1997; Mann, 1997), with the CDC (Centers for Disease Control) report about the occurrence, without identifiable cause, of PCP (formal *Pneumocystis carinii* pneumonia, now *Pneumocystis jiroveci* pneumonia) in five previously healthy gay men in Los Angeles (Schamatz *et al*., 1990; Wakefield *et al*., 1992). Several other similar reports of PCP cases and other opportunistic infections among gay men, as well as of a rare and unusually aggressive cancer – the *Kaposi's sarcoma* – also reached the CDC. By the end of the year, there was a total of 270 reported cases of severe immune deficiency among gay men, and 121 of those individuals had already died. It was a period of general confusion and divergent conclusions about what this new disease was, how it was transmitted, and whom did it affect (http://www.avert.org; https://www.aids.gov).

The name AIDS was officially given by the CDC in 1982, as up until then organizations were referring to it in different ways: by reference to the diseases that were occurring (*e.g*. lymphadenopathy – swollen glands), "Gay Compromise Syndrome", GRID (Gay-Related Immune Deficiency), AID (Acquired Immunodeficiency Disease), "Gay Cancer" or "Community-Acquired Immune Dysfunction". The name was given in reference to it being acquired rather than inherited, because it resulted in a deficiency

within the immune system and because it was a syndrome, with a number of manifestations, rather than a single disease (http://www.avert.org).

AIDS took a turning point in people awareness when the first reports in children (by mother-child transmission) and in blood-transfusion recipients appeared. Up until then, non-gay people and non-drug injectors felt unthreatened by it. As Harold Jaffe *apud* http://www.avert.org stated, in the CDC for Newsweek Magazine, "*Up until then it was entirely a gay epidemic, and it was easy for the average person to say 'So what?' Now everyone could relate*."

In 1983, doctors at the Institute Pasteur in France reported that they had isolated the Lymphadenopathy-Associated Virus (LAV), which they suggested might be the cause of AIDS, but little notice was given to it (Barré-Sinoussi *et al*., 2013). A year later, Dr. Robert Gallo, of the National Cancer Institute, announced that he had also isolated the virus which caused AIDS, and named it HTLV-III. Later it became clear that they were the same virus. To end the general discussion on its name, the International Committee on the Taxonomy of Viruses attributed a new name – HIV (http://www.avert.org/).

In April 1985, the first international conference on AIDS was held in Atlanta. Immediately after, the World Health Organization (WHO) organized an international meeting to consider the AIDS epidemic and to initiate intensive worldwide action. The WHO's Global program on AIDS was then created in 1986-1987 (Kaiser Family Foundation, 2015; WHO, 1997) in order to prevent infection of HIV, to reduce its personal and social impact and to mobilize national and international efforts to combat AIDS (WHO, 1997, Mann, 1997). By then, approximately 75,000 cases had been reported to WHO (WHO, 1997).

Meantime, a second parallel "epidemic of fear" and prejudice was rising within many countries, with the increasing numbers of infected and dying people and the lack and/or misinformed knowledge from the epidemic. Many campaigns against discrimination and promoting AIDS awareness arose, and the AIDS-related organizations raised efforts to educate people (http://www.avert.org/).

As the virus had yet to be stopped, in 1996, UNAIDS (Joint United Nations Program on HIV/AIDS) was formed to serve as the UN (United Nations) system's coordinating body and to help galvanize worldwide attention to AIDS (Kaiser Family Foundation, 2015).

In 2000, all nations agreed to 10 goals to be met until 2015 regarding several of the most serious diseases worldwide – the UN Millennium Development Goals (MDGs). The 6th goal regarded several HIV/AIDS targets. In the UNAIDS 2015 report it was stated that they all have been met (Kaiser Family Foundation, 2015; UNAIDS, 2015).

In 2001, a United General Assembly Special Session on HIV/AIDS (UNGASS) was assembled and the Global Fund was created (Kaiser Family Foundation, 2015; UNGASS, 2001). In the 2011 UNGASS meeting, world leaders adopted a new Political Declaration on HIV and AIDS that reaffirmed

commitments and appealed for an intensification of efforts to combat the epidemic through a total of 10 targets to be met by 2015 (Kaiser Family Foundation, 2015; United Nations, 2011).

In World AIDS Day 2014, UNAIDS set targets for 2020 aimed at ending the epidemic by 2030 (Kaiser Family Foundation, 2015; UNAIDS, 2014).

By the end of 2014, there were approximately 36.9 million people living with HIV. In that same year, there were 2.0 million new HIV infections and 1.2 million AIDS-related deaths globally (UNAIDS, 2015; WHO, 2015).

b. HIV infection

The HIV is a lentivirus[1] belonging to the family Retroviridae[2] that causes HIV infection, which might evolve into AIDS in later stages of the infection. Two HIV strains have been identified: HIV-1 (more virulent; major responsible of AIDS) and HIV-2 (less common) (Goede *et al.,* 2014).

Each HIV particle (Fig. 1) is composed of three major elements: i) an outer coat composed of a lipid bi-layered envelope that comprises viral glycoproteins, ii) an associated matrix surrounding the capsid that ensures the integrity of the virus particle, and iii) an inner core enclosing two identical copies of a single-stranded RNA genome (9600 nucleotides), polymerase and additional viral proteins, packaged by the nucleocapsid (Goede *et al.,* 2014). HIV encodes for nine protein classes: three structural proteins, two regulatory proteins (Tat and Rev) and four accessory proteins (Vif, Vpu, Nef and Vpr). The structural protein classes consist of Gag (capsid proteins), Pol (viral enzymes protease, reverse transcriptase and integrase) and Env (envelop proteins) (Goede *et al.,* 2014; Peçanha *et al*., 2002).

[1] Long incubation periods, infect non-dividing cells.
[2] Enveloped viruses that replicate in the host cell via the enzyme reverse transcriptase to produce DNA from its RNA genome (Goede *et al*., 2014).

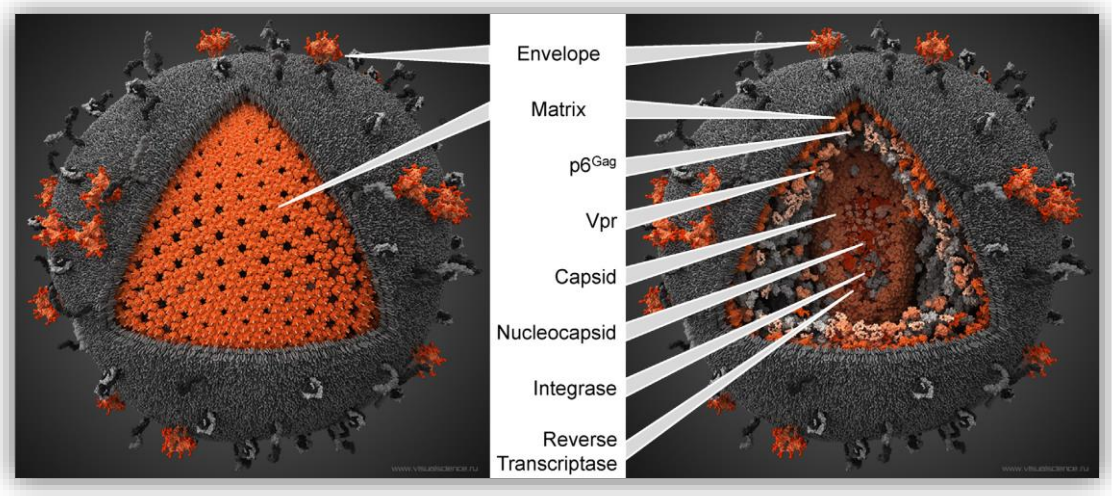

Figure 1 – Illustrations of a 3D representation of a HIV-1 virion. Viral proteins in red/orange, host proteins in black/grey. *Illustration adapted from https:// www.visualscience.ru.*

HIV infection is characterized by CD4 T lymphocytes cell (T cells) depletion, CD8 T cell expansion and chronic immune activation that leads to immune dysfunction (Catalfamo *et al*., 2011). HIV mainly targets CD4 T cells, macrophages, monocytes and dendritic cells, as HIV entry depends on the presence of certain surface receptors (majorly CD4) and co-receptors (Goede *et al*., 2014).

HIV can be transmitted through sexual contact, blood transfusion, organ transplant, parenteral drug use, mother to child (either during pregnancy, childbirth or breast feeding) or by any other type of fluids (semen, pre-seminal fluid, rectal and/or vaginal fluids, blood, breast milk) exchange (https://www.aids.gov).

When HIV enters the body, it first attaches to the dendritic cells, found in the mucosal membranes. The dendritic cells then transport the virus from the site of infection into the lymph nodes, where HIV can then infect other immune system cells (https://www.aids.gov).

The HIV replication cycle (Fig. 2) starts with the virus binding to the CD4 receptor and co-receptors of the host-cell, which results in cell and viral membranes fusion. The virion is then uncoated and its contents – RNA and proteins – are released into the cytoplasm. The HIV RNA is reverse transcribed into cDNA by the viral enzyme reverse transcriptase and the pre-integration complex assembles and goes to the nucleus. Once there, the viral cDNA is integrated into the host DNA, by the viral enzyme integrase, and subsequently transcribed and translated to form new viral RNA and viral proteins. These translocate to the cell surface to assemble into new immature virus forms that bud off and get released. Afterwards, the new viruses suffer maturation, where the viral protease enzyme cleaves structural proteins present in the envelop, and they finally convert into mature viruses fully capable of infecting new cells (Barré-Sinoussi *et al*., 2013; Goede *et al*., 2014).

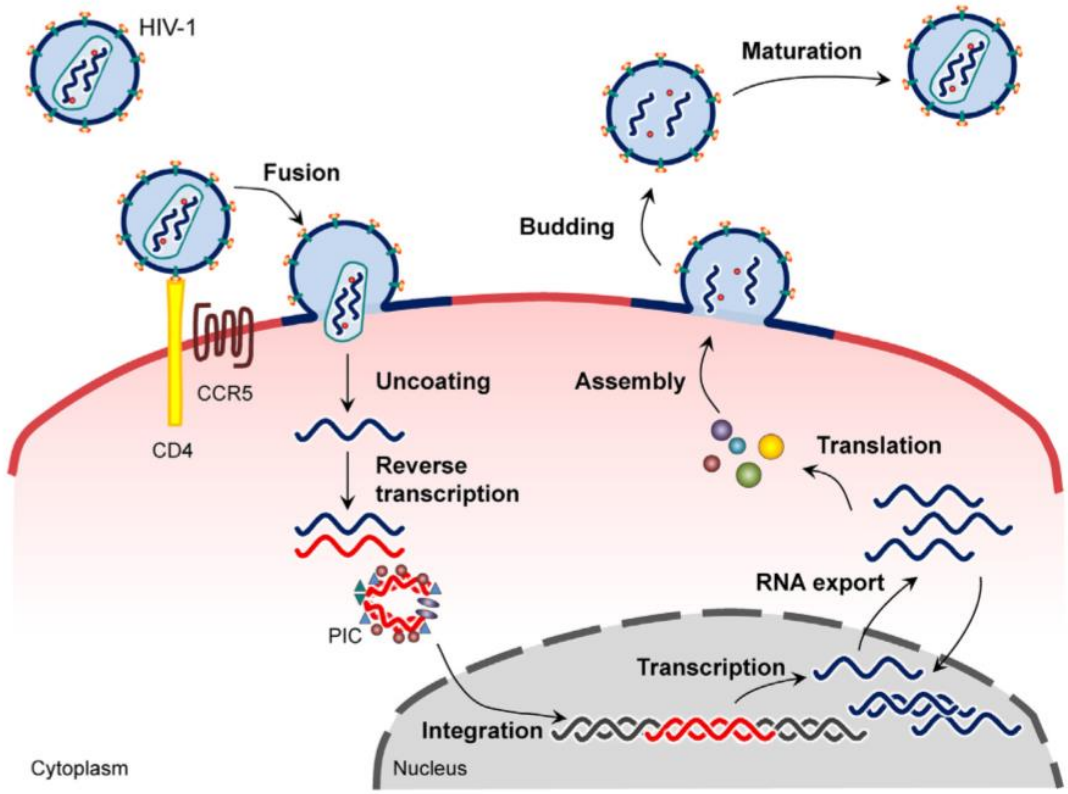

Figure 2 – HIV replication cycle. The main steps of the replication cycle are shown: binding to the CD4-receptor and co-receptors; fusion with the host-cell membrane; uncoating of the viral capsid; release of the viral genome and proteins into the cytoplasm; reverse transcription of the RNA into DNA; formation of the pre-integration complex; translocation into the nucleus. The viral DNA is then integrated into the host DNA and is transcribed inside the nucleus. After export, RNA is translated to form new viral RNA and viral proteins that assemble at the host-cell membrane. New immature viruses bud from the host-cell and are released after which they mature, resulting in the production of new infectious virions. *Illustration adapted from Goede* et al. *(2014).*

As the number of CD4 cells depletes, resulting in a dysfunctional immune system, the risk of contracting OIs and certain cancers increases gigantically. When patients get a very low number of CD4 T cells (below 200 cells/mm^3), have one or more of the 20 OIs listed by WHO and/or have certain cancers, they are considered to have progressed into AIDS. OIs are the most common cause of death of HIV infected patients that are not receiving therapy (https://www.aids.gov/).

c. Treating HIV/AIDS

Despite all the efforts and mutual aid between nations, a vaccine and/or cure for HIV/AIDS as yet to be found (Walker and Burton, 2008; Richman *et al*., 2009). There are, though, several studies being made towards it (rgp120 HIV Vaccine Study Group, 2005; Walker and Burton, 2008) and enormous progresses have been made in order to slow the spread of HIV, prevent new infections and to improve the quality of life and life expectancy of people living with AIDS, and those are not to be discarded (Richman *et al*., 2009). The discovery and following implementation of Antiretroviral Therapy[3] (ART) made it possible.

The first antiretroviral (ARV) drug that showed signs of slowing down the attack of HIV, the Azidothymidine (AZT), appeared in September 1986. After a quick clinical trial, as it was considered unethical to provide placebo to the patients and deny them the medicine, the U.S. Food and Drug Administration (FDA) approved AZT and it started to be commonly given to AIDS patients (http://www.avert.org).

In 1992, the FDA approved the use of the first successful antiretroviral combination therapy for the treatment of AIDS – dideoxycytidine plus AZT – for adult patients with advanced HIV infection who were continuing to show signs of clinical or immunological deterioration (http://www.avert.org).

In 1995, FDA approved the first protease inhibitor, the drug saquinavir. This new class of drugs proved to be very potent, such as that this announcement was considered one of the best news for people living with AIDS (http://www.avert.org).

By 1997, it was common for the therapy against HIV infection to be held by at least 3 ARVs. This combination therapy was referred as Highly Active Antiretroviral Therapy (HAART) or simply by ART (Berns and Kasbekar, 2006; Kalyesubula and Perazella, 2011; WHO, 2013; http://www.avert.org).

The figure 3 displays the timeline of the introduction of ARVs.

[3] Therapy held by a combination of 3 or more ARVs (WHO, 2013); it might also be referred as HAART (Berns and Kasbekar, 2006; Kalyesubula and Perazella, 2011).

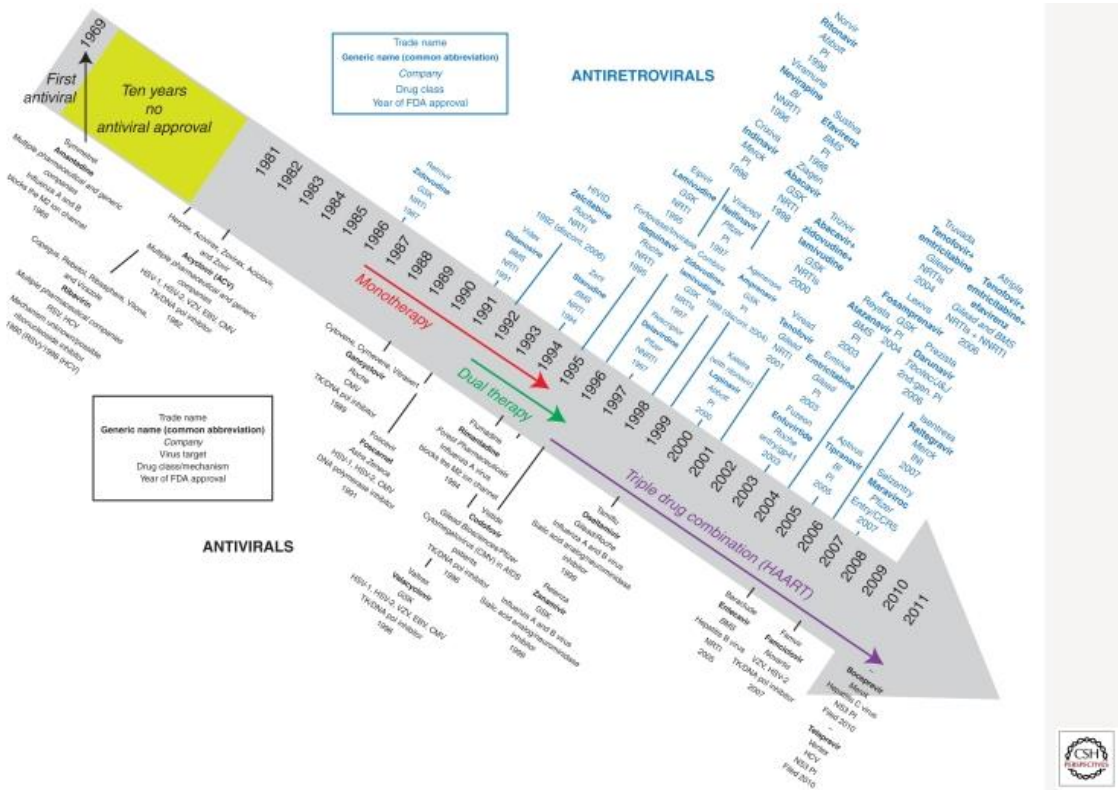

Figure 3 – Timeline of the appearance of new ARVs, as they were being approved by the FDA.

Now, more than 20 ARVs are available and they can be combined in several different ways (Berns and Kasbekar, 2006). Each drug can block one of the steps of the HIV viral cycle. They are distributed in five different classes, according to the step of the viral cycle they target ant their mechanism of action (Arts and Hazuda, 2012; https://aidsinfo.nih.gov):

- Nucleoside Reverse-Transcriptase Inhibitors (NRTIs) are nucleoside or nucleotide analogues (*e.g.* Tenofovir) administered in the form of pro-drugs, requiring triple or double phosphorylation by cellular kinases before enacting an antiviral effect. When incorporated into the new forming cDNA chain, they prevent the incorporation of new nucleosides and thus terminate with the synthesis of the viral DNA;
- Non-Nucleoside Reverse-Transcriptase Inhibitors (NNRTI) are non-competitive inhibitors that bind allosterically to the reverse transcriptase, preventing HIV replication;
- Protease Inibitors (PIs), as the name indicates, block protease, preventing HIV viral polyprotein processing and thus maturation of new (immature) HIV;
- Integrase Strand Transfer Inhibitor (INSTI) block integrase, preventing proviral cDNA from integrating into the cell genome;
- Entry inhibitors:
    - Fusion Inhibitors block the HIV envelope fusion with the host CD4 cell membrane, preventing the viral RNA and proteins from entering the cell;

- CCR5 Antagonists block the CCR5 co-receptor on the surface of CD4 cells, preventing HIV from entering the cell.

ART act by gradually restoring pathogen-specific immune responses, mediated by a suppression of HIV replication and an increase in the CD4 cell count. However, many patients in resource-poor settings start ART at late stages of the disease, thus decreasing the benefic effects of the treatment (Muller *et al*., 2010). Other barriers, such as a poor adherence and non-persistency of the therapy, insufficient clinical surveillance and viral resistance may also explain the sometimes inefficient therapy treatment (Bae *et al*., 2011).

According to the most recent WHO 2013 Treatment Guidelines (WHO, 2013), HIV-infected people should undergo ART treatment when CD4 cell count is lower than 500 cells/mm^3. Current guidelines (WHO, 2013; Panel on Antiretroviral Guidelines for Adults and Adolescents, 2015) recommend as first line ART a combination of 2 NRTIs plus 1II or 1 PI (Table 1).

Table 1 – Recommended, Alternative, and Other Antiretroviral Regimen Options for Treatment-*Naïve* Patients. *Adapted from Panel on Antiretroviral Guidelines for Adults and Adolescents (2015).*

Recommended Regimen Options (Drug classes and regimens within each class are arranged in alphabetical order.)
INSTI-Based Regimens: • DTG/ABC/3TC[a]—**only** for patients who are HLA-B*5701 negative **(AI)** • DTG plus TDF/FTC[a] **(AI)** • EVG/c/TDF/FTC—only for patients with pre-treatment estimated CrCl ≥70 mL/min **(AI)** • RAL plus TDF/FTC[a] **(AI)** PI-Based Regimens: • DRV/r plus TDF/FTC[a] **(AI)**
Alternative Regimen Options (Drug classes and regimens within each class are arranged in alphabetical order.) Regimens that are effective and tolerable, but that have potential disadvantages when compared with the recommended regimens listed above, have limitations for use in certain patient population, or have less supporting data from randomized clinical trials. **An alternative regimen may be the preferred regimen for some patients**.
NNRTI-Based Regimens: • EFV/TDF/FTC[a] **(BI)** • RPV/TDF/FTC[a]—**only** for patients with pre-treatment HIV RNA <100,000 copies/mL and CD4 cell count >200 cells/mm^3 **(BI)** PI-Based Regimens: • ATV/c plus TDF/FTC[a] —**only** for patients with pre-treatment estimated CrCl ≥70 mL/min **(BI)** • ATV/r plus TDF/FTC[a] **(BI)** • (DRV/c or DRV/r) plus ABC/3TC[a] —**only** for patients who are HLA-B*5701 negative (**BIII** for DRV/c and **BII** for DRV/r) • DRV/c plus TDF/FTC[a] —**only** for patients with pre-treatment estimated CrCl ≥70 mL/min **(BII)**

Before ART, life expectancy was measured in months; now it is measured in decades. Besides, nowadays HIV viral load can be suppressed to undetectable levels (Berns and Kasbekar, 2006).

In 2000, less than 700,000 people were receiving antiretroviral drugs; by 2014, 15 million people had access to it. In just 15 years, the number of new HIV infections reduced from around 3.1 million to around 2.0 million, thanks to the ART (Fig. 4.1). Without it, 30 more million people would have been infected with HIV and 7.8 million more would have died (Fig. 4.2) (UNAIDS, 2015).

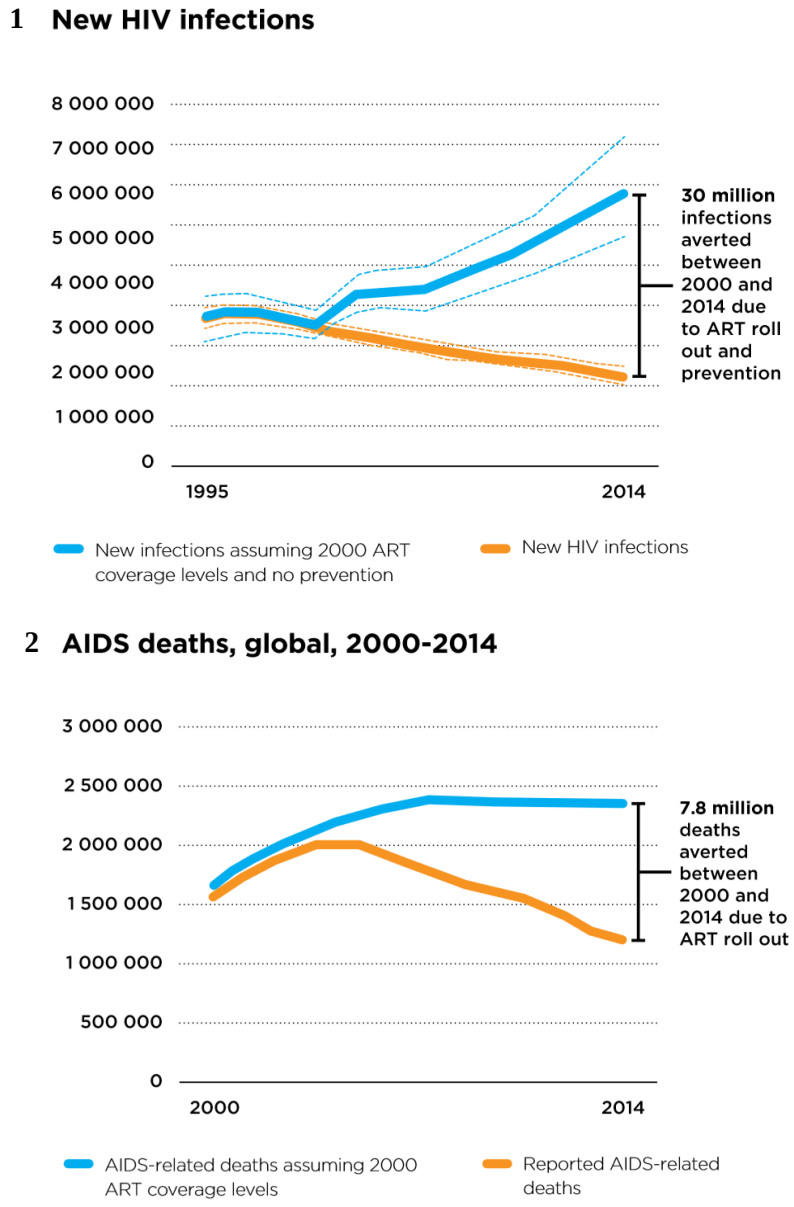

Figure 4 – Last statistics regarding HIV infection and ART impact on it. (1) New HIV infections, from 1995 till 2014. (2) AIDS related deaths, globally, from 2000 till 2014. *Illustrations adapted from UNAIDS (2015).*

d. ART associated toxicity

Even though the ART has prevented over 7.8 million deaths (Fig. 4.2) and has significantly increased the life-span of people living with AIDS from months to decades (UNAIDS, 2015), it has also been highly associated with mild to severe levels of toxicity. Because of the seriousness of the epidemic, the FDA has "rushed" the release of several new ARVs, with the approval of new regulations, in 1988, but many times without the proper long-term side effects studies been made on the new drugs (http://www.avert.org/).

By 1997 doctors were becoming increasingly aware of the unpleasant and sometimes serious side effects of these drugs and several "post-market" studies appeared later reporting serious side effects of some drugs (http://www.avert.org/).

Regarding ARVs associated nephrotoxicity, it is important to highlight that HIV by itself has always been associated with renal complications, as the virus can cause direct injury to the kidneys, a condition referred as HIV-associated nephrotoxicity (HIVAN) (Kalyesubula and Perazella, 2011). Other forms of HIV-related nephropathies include HIVICK (HIV Immune-Complex Kidney Disease), HIV thrombotic microangiopathy and kidney disease associated with opportunistic infections, such as cytomegalovirus, mycobacterium, cryptosporidium, and malignancies like lymphoma and Kaposi's sarcoma (Gerntholtz *et al*., 2006; Tambkus *et al*., 2006; Brady *et al*., 2010; Pollol *et al*., 1995). Also, Hepatitis B and C infections, often related and present in HIV infected people, also contribute to several glomerular lesions (Wyatt *et al*., 2008; Fischer *et al*., 2010; Szczech *et al*., 2004).

The kidney plays a major role in the metabolism and excretion of ARVs (Berns and Kasbekar, 2006; Kalyesubula and Perazella, 2011). For that reason, the kidney is a vulnerable target to many various types of injuries caused by ARVs, including acute kidney injury (AKI), tubulopathies, chronic kidney disease (CKD), and end-stage renal disease requiring renal replacement therapy (Kalyesubula and Perazella, 2011). HIV-infected people have a 3.87% increase risk of developing renal disease when compared to non-infected (Islam *et al*., 2012)

For that reason, nowadays HIV continues to be greatly associated with nephrotoxicity, but now majorly because of ART, as some ARVs cause renal toxicity (Kalyesubula and Perazella, 2011). ART related nephrotoxicity accounted for 14% of late-AKI episodes, occurring 3 months after initiating ART (Roe *et al*., 2008). CKD has also been associated with ART. In 3316 ART-naïve adults who were initiated with ART, 2.7% developed severe kidney dysfunction (Reid *et al.*, 2008).

It is difficult, though, to distinguish between ART-related and HIV-related kidney disease. And this challenge has now been increased by the fact that since HIV-patients are living longer, age-related kidney disease has also been included (Kalyesubula and Perazella, 2011). Deeks (2011) have reported

an interesting study relating common age-related diseases with HIV infection, suggesting that HIV patients may suffer from accelerated or premature "aging".

Therefore, the Infectious Disease Society of America *apud* Kalyesubula and Perazella (2011) recommends that all patients at the time of HIV diagnosis have to be assessed for existing kidney disease with a screening urine analysis for proteinuria and an estimate of the glomerular function in order to individualize the therapy. The most accurate method to measure GFR (Glomerular Filtration Rate) involves the administration of a substance like inulin or radio-isotopes that the glomeruli will filter completely as waste, without reabsorption nor secretion by the tubules, and measuring its clearance over time (Levey *et al*., 2002; Smith *et al*., 1951). Serum creatinine, albeit a classical method used to measure GFR, is believed to be a poor marker of renal disease, especially in patients with muscle wasting (Berns and Kasbekar, 2006), since several antiretroviral drugs, such as tenofovir, cause nephrotoxicity without impairment of the glomeruli.

Some drugs, thought, seem to be more closely related to kidney disease events. Islam *et al.* (2012) published a systematic review and meta-analysis of relative risk of renal disease among populations of people living with HIV. They reported an increased risk of renal disease of 0.54% among people undergoing ART therapy versus ART-*naïve* and an increased risk of renal disease of 1.56% among people receiving a tenofovir-based ART therapy versus non-tenofovir ART therapy.

e. Tenofovir

Tenofovir is one of the most used ARVs for the treatment of HIV infection, due to its easy administration, that enables for a high adherence, and high antiretroviral efficacy (Winiarczyk *et al*., 2009; Abraham *et al*., 2013). Tenofovir, a NRTI, is now part of the majority of ART therapies, besides being also a component of hepatitis B treatment (Fernandez-Fernandez *et al*., 2011).

Tenofovir bioavailability as tenofovir monophosphate (TFV) is relatively low, though, since it has a low oral absorption due to its non-ionic state that results in a low permeability across membranes (Gelder *et al.*, 2001). Therefore, it is administered as tenofovir disoproxil fumarate (TDF), a bi-ester oral pro-drug (Abraham *et al.*, 2013).

TDF is orally administered and absorbed by the intestinal tract. After being absorbed, TDF is degraded to its (mono)ester-equivalent, by carboxylesterases, and further to TFV, probably by phosphodiesterases, in the intestinal lumen (Fig. 5) (Gelder *et al*., 2001).

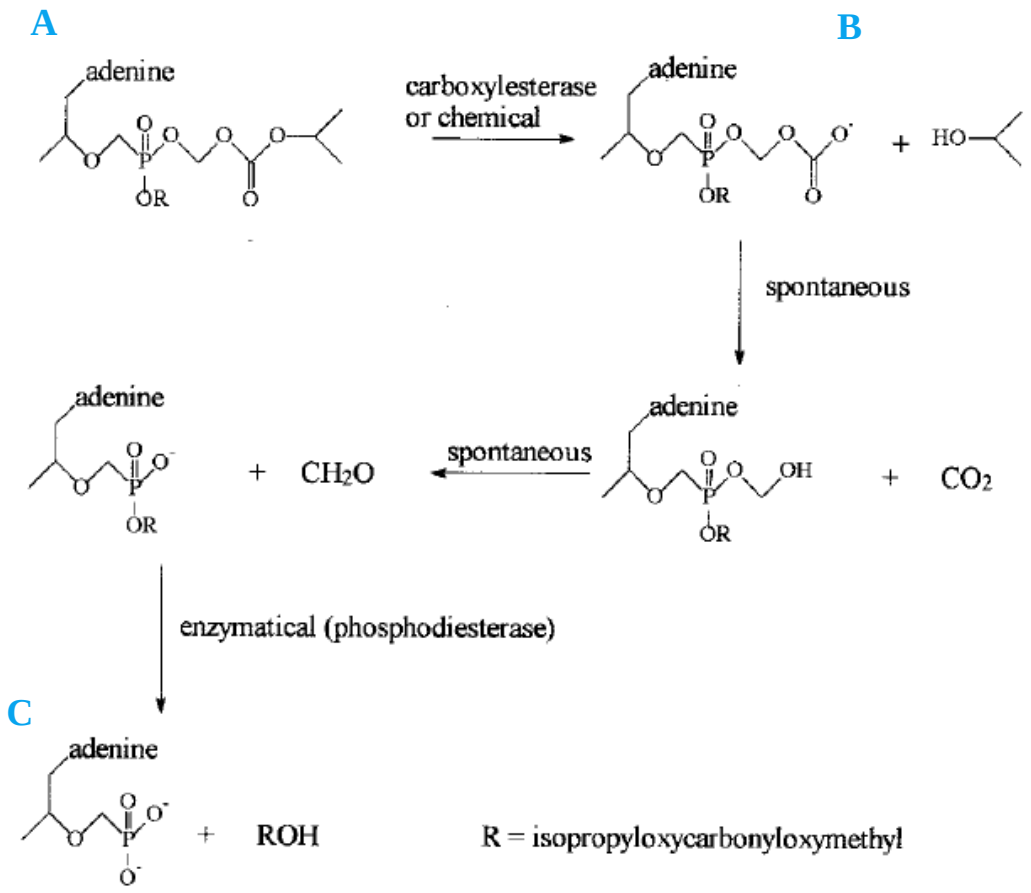

Figure 5 – Conversion of TDF to TFV. First, TDF (A) is converted to the (mono)ester intermediate (B) [enzymatically (mainly by carboxylesterases) or chemically] and further to TFV (C) (probably mediated by phosphodiesterases). *Illustration adapted from Gelder* et al. *(2002).*

TFV is then distributed across several tissues, majorly through the liver, kidney and intestines. TFV is eliminated unchanged through the kidneys, by glomerulus filtration and proximal tubules secretion (Fernandez-Fernandez *et al.*, 2011). 20-30% of the drug enters the proximal tubule cells by organic anion transporters (OAT1 and OAT3) in the basolateral membrane, and is secreted into the urine by apical membrane transporters (MRP4 and MRP2) (Fig. 6) (Moss *et al*., 2014; Fernandez-Fernandez *et al.*, 2011).

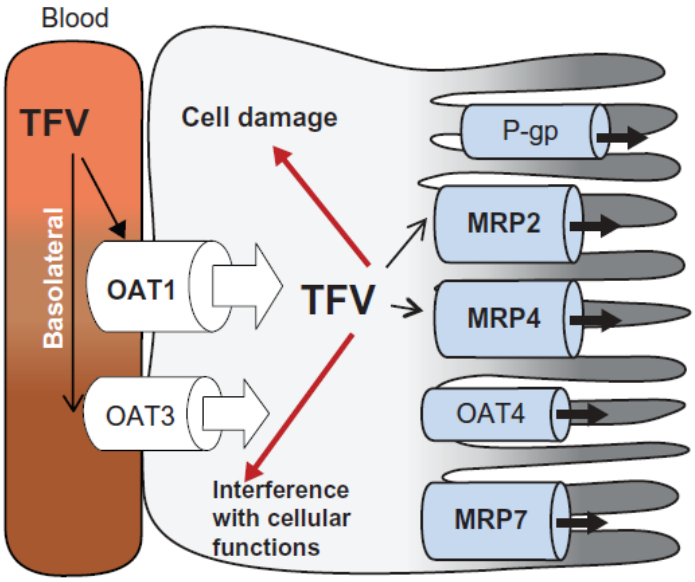

Figure 6 – Mechanism of TFV tubular secretion a tubular cell. *Illustration adapted from Novoa* et al. *(2011).*

TFV, after entering into the lymphocytes in order to exercise its antiretroviral activity, suffers two phosphorylations by cellular enzymes to give its antiretroviral-active form, tenofovir diphosphate (TD) (King *et al.* 2006). TD is a structural analog of deoxyadenosine-5'-triphosphate, the natural substrate for viral RNA-directed DNA polymerase, and is a weak inhibitor of mammalian DNA α- and β-polymerases and mitochondrial DNA γ-polymerase (Fernandez-Fernandez *et al.*, 2011).

When tenofovir first became available, early randomized clinical trials and post-marketing data supported the safety of tenofovir, as in none was observed Fanconi syndrome[4] nor drug discontinuation because of renal complications (Gallant *et al.*, 2004; Nelson *et al.*, 2007). It was only later that the first tenofovir-related nephrotoxicity studies started to arise. These mismatched results may be because clinical trials have very strict inclusion and exclusion criteria, while in routine clinical practice patients have highly diverse backgrounds, and some of them may be predisposed to a higher tenofovir nephrotoxicity sensibility (Fernandez-Fernandez *et al.*, 2011).

The main site of tenofovir toxicity is the proximal tubule. Since tenofovir has to enter the proximal tubular cells to be secreted, it accumulates inside them, causing toxicity. Current evidence suggests that mitochondria are the main targets of tenofovir toxicity within the cell. Several human (Tsai *et al.*, 2014) and animal studies have shown damage to specifically renal proximal tubular mitochondria (Abraham *et al.*, 2013).

[4] Characterized by phosphaturia, glycosuria, bicarbonate wasting, tubular proteinuria, and aminoaciduria (Abraham *et al.*, 2013).

It is well known that mitochondrial damage usually results in the overproduction of reactive oxygen species (ROS) and reactive nitrogen species (RNS), which upon accumulation can cause oxidative and nitrosative damage to the lipids, proteins and DNA. Proximal tubular cells have a relative high requirement for ATP for the active reabsorption of filtered nutrients and ions, making them naturally sensible to mitochondria damage, given the fact that mitochondria are the main producers of ATP in the cell (Abraham *et al*., 2013; Ramamoorthy *et al.*, 2014). Therefore, when mitochondria are impaired, ATP production is depleted and tubular cells cannot properly ensure reabsorption of ions and small molecules, such as potassium, glucose, phosphate, uric acid, amino acids, and β2- microglobulin. As it is, these molecules are secreted in abnormal quantities in the urine, which is the definition of the Fanconi syndrome (Tsai *et al*., 2014). Damage to the proximal tubular mitochondria can therefore have two consequences: i) proximal tubular dysfunction resulting in Fanconi syndrome and ii) increased production of ROS thereby resulting in increased oxidant stress (Abraham *et al.*, 2013).

The main clinical presentations of tenofovir nephrotoxicity are: i) proximal tubular dysfunction with normal renal function and ii) proximal tubular dysfunction with decreased renal function. Decreased renal function may be classified as AKI, CKD, or GFR that is decreased when compared with baseline values, albeit within normal limits. In severe cases patients can develop Fanconi syndrome that may or may not be associated with decreased GFR (Abraham *et al*., 2013; Fernandez-Fernandez *et al*., 2011). Tubular dysfunction may precede the decline of renal function (Fernandez-Fernandez *et al*., 2011). Thus, it is important to highlight that tenofovir associated nephrotoxicity not always is associated with altered GFR, one of the mostly used parameters that is routinely checked for the diagnosis of kidney diseases.

As with most drugs, the prediction and management of tenofovir-related neuphrotoxicity has been relying on the mechanisms of the drug insult and on optimal animal models to explore it. Albeit several case reports and meta-analyses have been performed on humans, they have important limitations due to the big number of factors that cannot be controlled over the population, *e.g*. genetic factors, environment factors (*e.g.* diet, alcohol, smoke, drugs), low adherence to the therapy, alterations of prescribed ARVs mid-therapy (mainly because of its ineffectiveness and/or side effects) (Islam *et al*, 2012). As it is, animal models are indispensable for the study and understanding of diseases and new drugs that arise to combat it.

2. *Zebrafish (*Danio rerio*)*

Several different animal models have been used to date – rats, mice, mini-pigs, fruit flies and others in toxicology (Kohler *et al.*, 2009; Ramamoorthy *et al*., 2014; Cui *et al*, 2014; Cud, 2005). The animal model may vary depending of the study intent and field area, but an emergent animal model to study drug toxicity that has been gaining popularity, given its attractive advantages is the zebrafish.

a. Ecology

Kingdom: Animalia

Phylum: Chordata

Superclass: Osteichthyes

Class: Actinopterygii

Order: Cypriniformes

Family: Cyprinidae

Genus: *Danio*

Species: *D. rerio*

The zebrafish (*Danio rerio*) are ray-finned fishes (Actinopterygii), a class of the bony fishes superclass (Osteichthyes). They belong to the Cypriniformes order and to the family of freshwater fishes Cyprinidae (Spence *et al*., 2008).

Zebrafish are indigenous to South Asia, around the Ganges and Brahmaputra river basins, and are broadly distributed across parts of India, Bangladesh, Nepal, Myanmar, and Pakistan (Lawrence, 2007; Spence *et al.*, 2008) (Fig. 7).

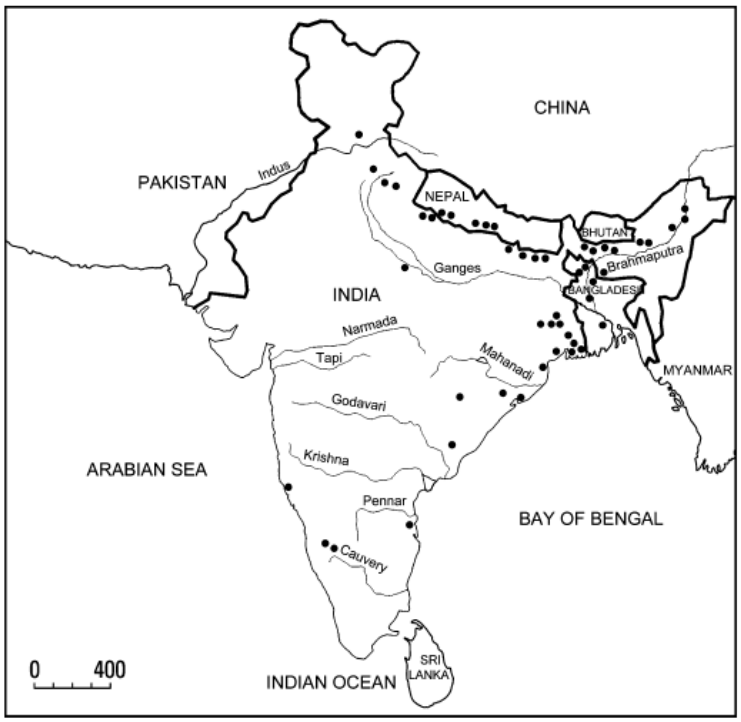

Figure 7 – The natural distribution of the zebrafish. Major river systems indicated. Black dots indicate recorded occurrences. *Illustration adapted from Spence* et al. *(2008).*

These reported natural occurrences suggest that zebrafish seem to prefer still or slow moving water bodies, for example the edges of streams and ditches, particularly adjacent to rice-fields (Sterba, 1962, Talwar & Jhingran, 1991; Jayaram, 1999), which are more likely free of large predatory fishes (Spence *et al.*, 2008) and rich in fertilizers that promote the growth of zooplankton, a major component of the zebrafish diet. They also prefer shallow waterbodies, frequently in unshaded locations with aquatic vegetation and a silty substratum (Spence *et al*., 2008). They have a preference for slightly alkaline water (pH~8.0) of relatively high clarity (Lawrence, 2007) and have a maximal thermal tolerance range of 6.7–41.7ºC, although the recommended temperature range for their maintenance, given by Matthews *et al.* (2002), is 24-30ºC.

Zebrafish are omnivorous, their natural diet consisting primarily of zooplankton and insects (Spence *et al.*, 2008). They are an annual species in nature (Spence *et al*., 2008), but domesticated zebrafish have been shown to have a mean life span of 42 months (Gerhard *et al.,* 2002). In the laboratory, domesticated zebrafish strains breed all year whereas in nature spawning is more seasonal, which is probably dependent on food availability that co-varies with season, since their natural habitat has a monsoon climate (Spence *et al.*, 2008). They have courtship behavior and ovulation is dependent on female exposure to male gonadal pheromones (Spence *et al.*, 2008).

Adult zebrafish rarely exceeds 40 mm Standard Length (from the tip of the snout to the origin of the caudal fin) and have a fusiform shape. Three types of pigmented cells are responsible for their color

pattern: dark blue melanophores, gold xantophores and iridescent iridophores. They have five to seven blue stripes that interleave with yellow ones (White *et al*, 2007; Spence *et al*., 2008) (Fig. 8).

Males and female fish are very similar, albeit males tend to be slimmer and have larger and more yellow anal fins, while females tend to have a bigger belly (Fig. 8).

Figure 8 – Male and female adult zebrafish. The fish on the top of the image is a male fish, while the bottom one is a female. *Image adapted from http://www.achetudoeregiao.com.br/.*

*b. Zebrafish (*Danio rerio*) as a powerful vertebrate model*

The zebrafish has emerged as an excellent model organism for studies on vertebrate biology. It is especially attractive due to its several advantages (Dooley and Zon, 2000; Bluthgen, 2014):

1. It is a vertebrate animal;
2. All sequenced genome;
3. High homology with humans at the genetic (85% of homology in genomes), anatomical, physiological, cellular and molecular levels;
4. Embryonic transparency, that allows a visual analysis of early developmental processes as well as microinjection;
5. Rapid development, with precursors of all major organs developed within 36 hours post fertilization (hpf) and fully developed larvae available after 48 - 72 hpf;
6. They achieve sexual maturity at 3-4 months;
7. Embryonic development outside the uterus;
8. Females are capable of spawning several hundred eggs every week, all year round;

9. Small and robust;
10. Low space requirements;
11. The different development stages are well characterized;
12. Wealth and versatility of genetic, cellular and physiological manipulations that can be performed;
13. Several different transgenic strains available;
14. Relativly cheap maintenance.

Therefore, several authors have searched and requested zebrafish to perform a high variety of studies, including nephrotoxicity tests, since the zebrafish kidney is now recognized as a valuable tool to identify and assess the function of renal genes and model renal diseases (Gerlach and Wingert, 2013), and the kidney is an organ highly susceptible to drug toxicity.

The vertebrate kidney is an essential organ responsible for the removal of metabolic waste through blood filtration. In addition, it also produces several important regulatory hormones and helps to maintain homeostasis (*e.g.*, fluid, pH, blood pressure) (Drummond and Davidson, 2010).

The kidney is composed of several nephrons, the functional units of the kidney. A nephron is composed of a glomerulus (the blood filter) attached to a segmental epithelial tubule that guides the filtrate – urine – into a collective duct and later to the urinary bladder for excretion (Drummond and Davidson, 2010; Cheng *et al*., 2015).

Higher vertebrate's embryo development is characterized, regarding kidney ontogeny, for the generation and subsequent degradation of three kidneys of increasing complexity. The first kidney-like structure is the pronephros, whose function in higher vertebrates, up until now, is not known. Upon its degradation, the mesonephros arises, who functions as the embryo filtration organ. The metanephros arises then, upon the mesonephros destruction, and serves as the adult kidney (Drummond and Davidson, 2010; Cheng *et al.*, 2015).

Lower vertebrates, such as the amphibians and fishes, never develop a metanephros, instead using the mesonephros as the adult kidney. Also, opposite to the higher vertebrates, its pronephros is fully functional and serves as the filtration and osmoregulation organ in free-swimming larvae (Cheng *et al.*, 2015; Drummond *et al.*, 1998).

The larvae zebrafish pronephros, opposite to the mesonephros and metanephros, is a very simple organ that is fully developed at 4 dpf (days post fertilization). It consists of only two nephrons with two glomerulus fused together at midline, pronephric tubules connecting directly to the glomeruli and paired bilateral pronephric ducts which conduct the filtrate outside the animal, through the cloaca (Drummond *et al.*, 1998) (Fig. 9.2). The tubular epithelium of the zebrafish pronephros is subdivided into two

proximal tubule segments (proximal convoluted tubule and proximal straight tubule) and two distal tubule segments (distal early and distal late) that are homologous in several ways to the segments of the mammalian nephron (Drummond and Davidson, 2010) (Fig. 9.3).

Although the overall structure of the zebrafish pronephros is quite different from higher vertebrate's kidney, tubular and glomerular differentiation processes are similar (Fig. 9.1) (Cheng *et al.*, 2015; Drummond *et al.*, 1998). Several reports have previously shown that the functions of many genes important during mammalian renal ontogeny are conserved in the zebrafish.

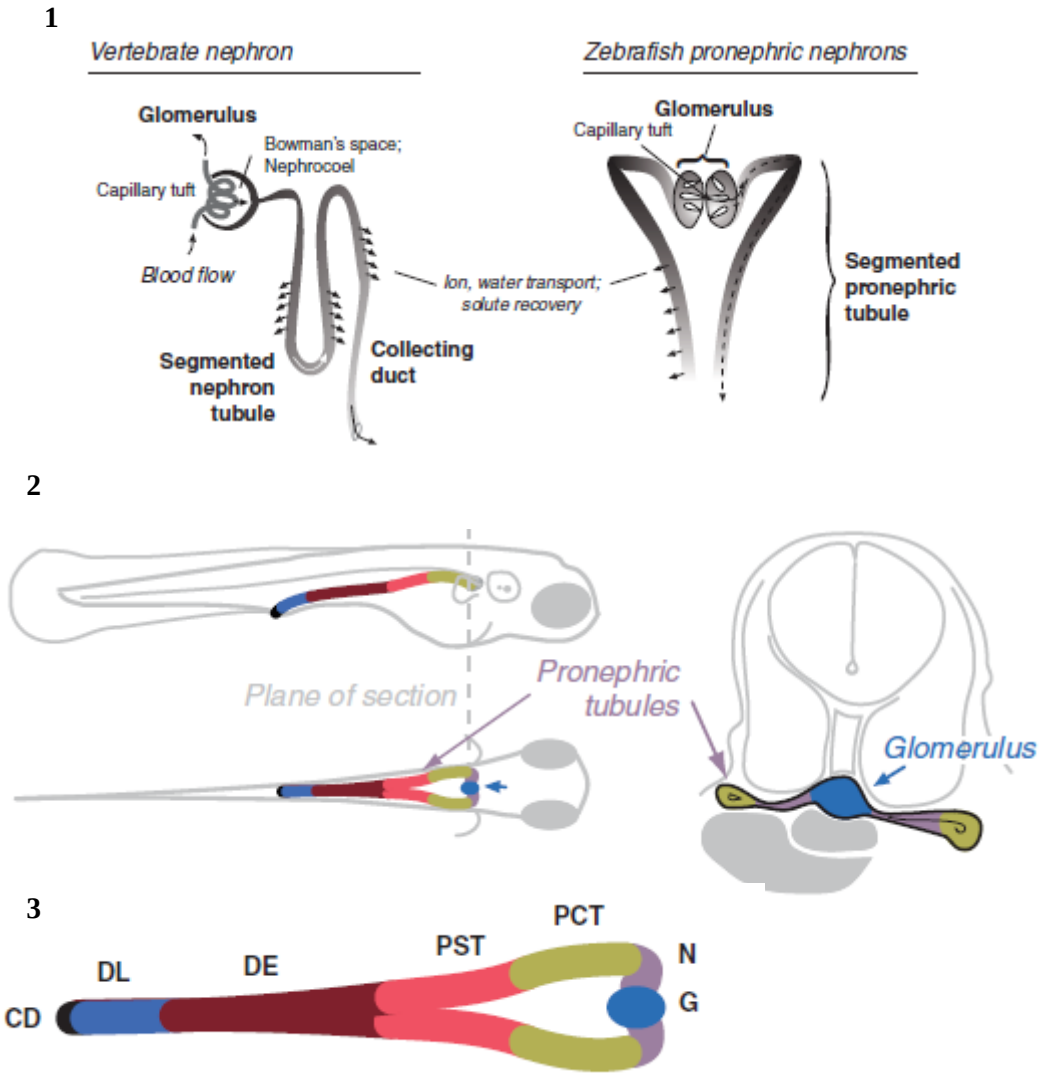

Figure 9 – Zebrafish pronephros. (1) Similarity between the vertebrate nephron and the zebrafish pronephric nephrons. (2) Diagram of the zebrafish pronephric kidney in a 3 dpf larva; midline compound glomerulus connects to the segmented pronephric tubules that run laterally; the nephrons are joined at the cloaca where they communicate with the exterior. (3) The several segments that comprise the zebrafish nephron: neck (N), proximal convoluted tubule (PCT), proximal straight tubule (PST), distal early (DE), late distal (DL), and collecting duct (CD). *Illustration adapted from Drummond and Davidson (2010).*

Therefore, the zebrafish is an attractive tool for the *in vivo* research on the regulation of kidney development, and has been quite useful in the study of the glomerulus formation, as well as on its molecular regulation. The zebrafish pronephros provides, then, a simplified renal system that can be used for the nephron-related studies, including nephrotoxicity.

Aims

What is known?

1. Zebrafish has become a very popular animal model in toxicology due to its several technical and scientific advantages;
2. Paracetamol and gentamicin, two drugs known to cause nephrotoxicity in humans, have already been demonstrated to cause morphological and/or functional alterations in the pronephros of zebrafish larvae;
3. Tenofovir, a widely used ARV, causes proximal tubulopathy that precedes the decline in the GFR;
4. The mechanism of renal toxicity of tenofovir is not fully understood, but mitochondria could be a possible target for its toxicity.

What needs to be known?

1. Whether zebrafish larvae are a good model to study tubular toxicity;
2. The relationship between tenofovir concentration and its lethality in zebrafish larvae;
3. If tenofovir affects the renal function in zebrafish larvae;
4. If tenofovir induces ultrastructural mitochondrial changes in zebrafish larvae;
5. It tenofovir induces mitochondrial DNA alterations in zebrafish larvae cells;
6. If there are any differences, in terms of toxicity, between tenofovir and its pro-drug, TDF.

Working hypothesis:

The working hypothesis of this thesis is that tenofovir induces the same alterations that are reported in humans, in zebrafish larvae: tenofovir causes mild or no alterations in the glomerular function and causes ultrastructural mitochondrial alterations in the proximal tubule.

Materials and methods

1. *Zebrafish lines used*

All procedures involving zebrafish were approved by the Ethical Committee at the Instituto Gulbenkian de Ciência (IGC), according with directives from Direcção Geral Veterinária (Portaria nº 1005/92 de 23 de Outubro).

For this work, two zebrafish lines were used: casper and nacre wt1b::GFP; cdh17::GFP. These specific lines were chosen because *nacre wt1b*::GFP; *cdh17*::GFP has the pronephros marked with green fluorescence and as the main focus of this thesis regards changes in this organ, it will prove to be helpful in further experiments; *casper* line was chosen because of the larvae transparency.

The *casper* (*mitfa*$^{-/-}$,*roy*$^{-/-}$) zebrafish are transparent through all adulthood and embryogenesis, since they are doubly mutant for *nacre* (complete lack of melanocytes due to a mutation in the *mitfa*[5] gene (Lister *et al*., 1999; White *et al.*, 2007) and *roy* (complete lack of iridophores, the gene/mutation responsible is currently unknown) (White *et al.*, 2007; http://zfin.org). This zebrafish line was chosen because its transparency allows to see the internal structures and organs of the larvae (including the blood vessels).

The *nacre* (*mitfa*$^{-/-}$, *roy*$^{+/+\ or\ +/-}$) *wt1b*::GFP*; cdh17*::GFP (Fig. 10.1) zebrafish are also transparent, since *nacre* zebrafish lack the *mitfa* gene, even though they express *roy*. The *Wilms tumor suppressor* (*Wt1b*) gene encodes a zinc-finger transcription factor and is expressed in several organs, such as the kidney, gonads and spleen (Horsfield *et al*., 2002). *cadherin-17* (*cdh17*). The zebrafish homolog of the mammalian kidney-specific *cadherin*[6], is expressed in the epithelium of the pronephric tubule and ducts, in larvae, as well as in the mesonephric tubules and ducts of juvenile fish (Zhou *et al*. 2010). In this line, the *wt1b* sequence is attached to the GFP sequence, thus driving the fluorescence expression to the proximal tubule and the glomerular *primordium* in the pronephros (Horsfield *et al*., 2002); another GFP sequence is attached to the promoter of *cdh17*, guiding the fluorescence to the distal and collecting ducts of the pronephros and mesonephros (Fig. 10.2). GFP is also expressed in the pancreas and gut, probably because of enhancer elements of the 5' neighbor gene of *wt1b*, the gene *ga17*, and also, more weakly, in the eye, gill arches and heart sac, due to the *wt1b*::GFP (Horsfield *et al*., 2002).

[5]*Microphthalmia-associated transcription factor a* (Lister *et al*., 1999).
[6]The cadherin superfamily of transmembrane glycoproteins are calcium-dependent cell adhesion molecules thatplay an active role in tissue morphogenesis and patterning (Zhou *et al*. 2010).

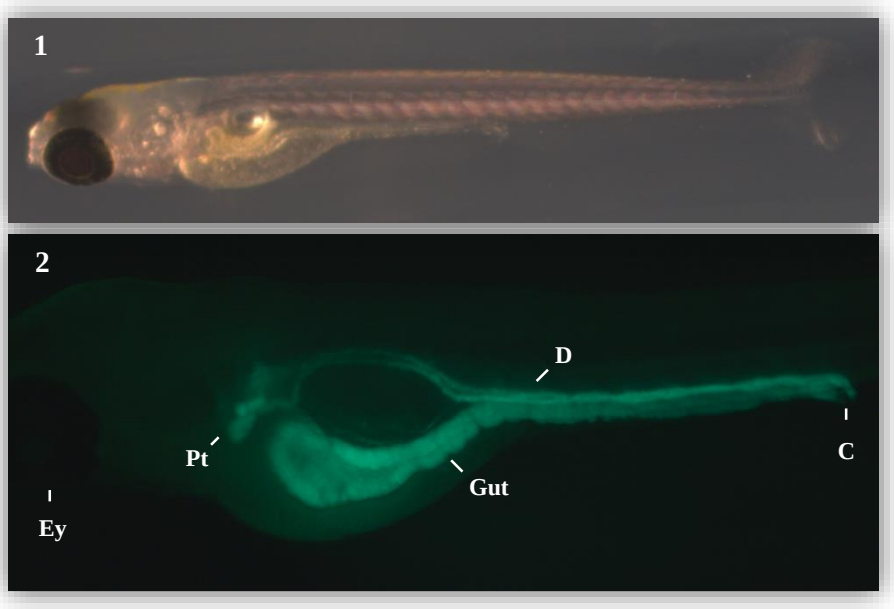

Figure 10 – 5 dpf *nacre* wt1b::GFP; cdh17::GFP larvae. (1) Whole larvae image, obtained with a microscope. (2) Close up of the region where the fluorescence can be seen, between the middle of the larvae eyes until the cloaca (from left to right); the image was obtained with a confocal microscope. Ey – eye; Pt – proximal tubule; D – duct; C – cloaca.

2. *Zebrafish breeding and maintenance*

Adult zebrafish were raised and maintained at 28ºC with 14h on/ 8h off light cycle, in the Fish Facility of the IGC. Male and female fish were matted once per week according to the protocols of the Fish Facility. After crossing, embryos were collected and grown at 28°C in embryo media (EM) till 4 dpf, time point when the zebrafish pronephros is structurally and functionally developed (Drummond *et al*., 2004). Embryo media was changed 24h after crossing in order to remove non-viable embryos.
All recipes of every solution can be consulted in the annex I.

3. *Drug stocks*

Three different drugs were used for the next experiments of this thesis: gentamicin, paracetamol and tenofovir. Gentamicin[7] and paracetamol[8] were used as positive controls, as several previous reports on zebrafish larvae stated that gentamicin decreased renal function (Hentschel *et al*., 2004) and paracetamol

[7] An aminoglycoside antibiotic used in the treatment of several bacterial infections manly caused by Gram-negative organisms (Perner *et al*. 2007).
[8] Also known as acetaminophen, is the most commonly available over-the-counter drug, and it is used for the relief of fever and headaches due to its analgesic and antipyretic properties (McCampbell and Wingert, 2014; David and Pancharatna, 2009)

induced morphological alterations in the glomerulus (Peng *et al*., 2010). Negative controls were exposed to the drug vehicle, water or EM. Tenofovir was administered in two forms: as TDF (Sequoia Research Products, UK) and TFV (Sequoia Research Products, UK). A stock solution for each drug was previously prepared at solubility concentration: 5000 µg/mL gentamicin, 12000 µg/mL paracetamol, 5000 µg/mL TFV and 6000 µg/mL TDF. All drugs powder were dissolved in water, except TFV, which was dissolved directly in EM due to its relatively low solubility and the high concentrations that are required to observe lethal effects. So, the percentage of water would be higher than the percentage of EM, which could be unpleasant to the larvae. All drug solutions were stored at -20ºC until further use.

4. Larvae drug exposition by soaking

Drugs were delivered by soaking, thus meaning by diluting a specific volume of each drug stock solution, or water or EM in case of negative controls, in the EM and in each well of a 96 well plate (total volume per well = 350 µL). 2 larvae of 4 dpf were placed per well. Drug exposition lasted 24h, at 28ºC. Larvae mortality and macroscopic alterations (including both behavioral and morphological alterations) were always registered.

5. Lethality curves

The *nacre wt1b::GFP; cdh17::GFP* zebrafish line was used to perform this experiment. Lethality curves for TDF and TFV were obtained with 5 or 6 different concentrations: 1000, 1500, 2000, 2500 and 3000 µg/mL for TDF and 2500, 3000, 3500, 4000, 4500 and 5000 µg/mL for TFV. Lethality curves for paracetamol and gentamicin had already been previously obtained. Drug concentrations for each drug were chosen so that the lowest would equal a 0% mortality and the highest a 100%. 10 larvae of 4 dpf were used for each concentration and 4 or 5 replicates were made for each drug concentration. After 24h of drug exposure, all zebrafish larvae were observed under a stereoscope (Nikon SMZ 745). The following characteristics were evaluated: body curvature, tail-flip response, heart oedema, heartbeat and necrosis. Lethality was defined as the absence of heartbeat and/or the presence of body necrosis. Percentages of lethality were calculated and plotted against the logarithm of drug concentration. The slope of the curves as well as the LC_{10} and LC_{50} (Lethal Concentration for 10% and 50% of the population, respectively) were calculated after the Probit transformation (Randhawa, 2009). The slope of each curve was obtained through the tendency line equation of the respective curve. The LC_{50} and LC_{10} values were obtained by plotting the probits values 5 or 3.72, respectively, against the log concentration.

The LC_{10} was the concentration selected for the following experiments of this thesis. Choice criteria were: i) high enough concentration that would probably enable the appearance of visible alterations, morphological and functional, with the different administrated drugs, and also ii) low enough concentration so that the majority of the living larvae would not be moribund, since it could give unreliable results and also because it would be unethical to keep the larvae in visible suffering with such high drug-toxicity levels.

6. FITC-inulin clearance assay

Renal function was assessed with the FITC-inulin clearance assay, following the protocol published by Rider *et al.* (2012), with some modifications. The *casper* zebrafish line was used for these experiments due to the transparency of their larvae and their non-fluorescence.

2.5% (w/v) FITC-inulin was dissolved in 0.9% NaCl, at ~70ºC, and dialyzed with 1000 Da dialysis tubing for the removal of any unbound FITC. The solution was stored at -20ºC until further use.

Casper larvae (4 dpf) were exposed to the LC10 of each drug for 24h. After drug exposition larvae were anaesthetized with a 1:6 dilution of tricaine (x25) and placed laterally on a 2% agarose injection mold. 1.4 nL of 2.5% (w/v) FITC-inulin solution, previously heated at ~70ºC to dissolve any potential crystals, was manually injected into the Common Cardinal Vein (CCV; formal Duct of Cuvier) (Fig. 11). ~15 min after injection, larvae were placed on a plain 2% agarose mold and initial FITC-intensity (0h) was captured by imaging laterally over the caudal region with a stereoscope (Zeiss Lumar, V12). The same magnification and fluorescence light intensity was applied for every image. After that, each larvae was placed individually in a well from a 96 black well plate with 100 µL EM. 2h later, each larvae was anaesthetized again and FITC-intensity was re-imaged. Larvae that had died in the meantime were discarded.

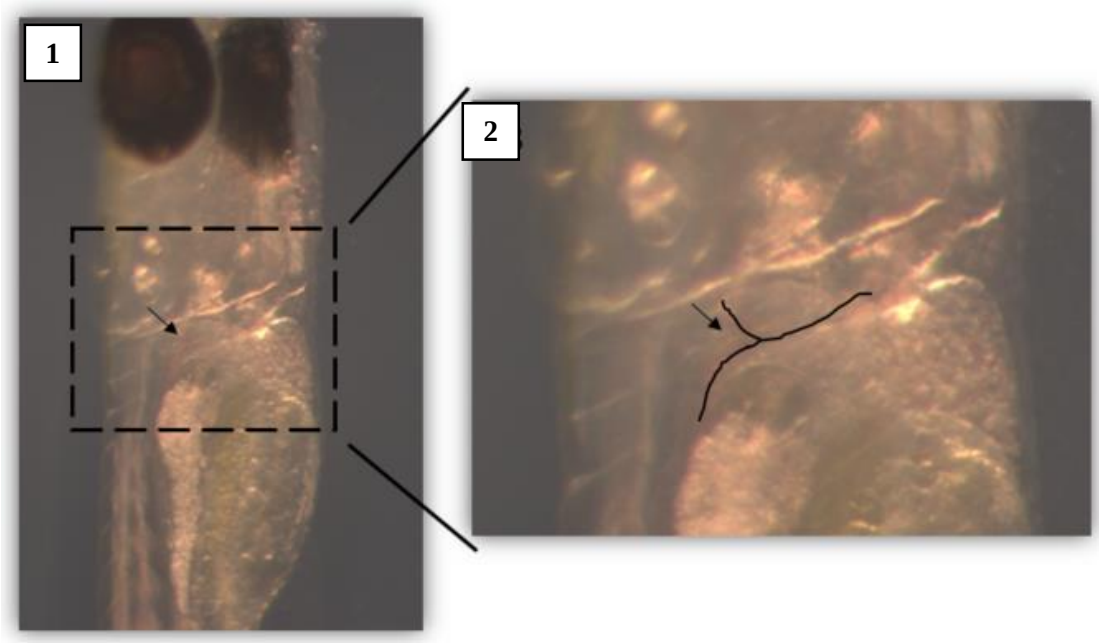

Figure 11 – Place of injection in larvae. Casper larvae (5dpf) were injected in the CCV, as part of the FITC-inulin clearance assay. (1) Larvae laterally placed upon an agarose mold. (2) Close up of the black dotted box of the previous image, showing the place of injection. Black arrows and line – CCV.

Fiji software was used to quantify FITC-intensity for each larvae. Rider *et al.* (2012) performed three FITC-intensity measurements over the caudal artery (Fig. 12.2), in the area posterior of the cloaca, between somites 16 and 18. But since this was a rather time consuming performance, Rider's protocol was adapted for the experiment reported here so that only one measurement was executed, covering the intersection of four intersegmental vessels (the area measured in Rider *et al.* (2012)) (Fig. 12.3). A paired-samples t-test (IBM SPSS v.22) confirmed the equality between the mean of the three FITC-intensity measurements and the one measurement made covering the same area of the caudal artery, for both the fluorescent values at 0h and 2h ($p<0.001$). As it is, the FITC-intensity was obtained by only one measurement throughout the rest of the experience.

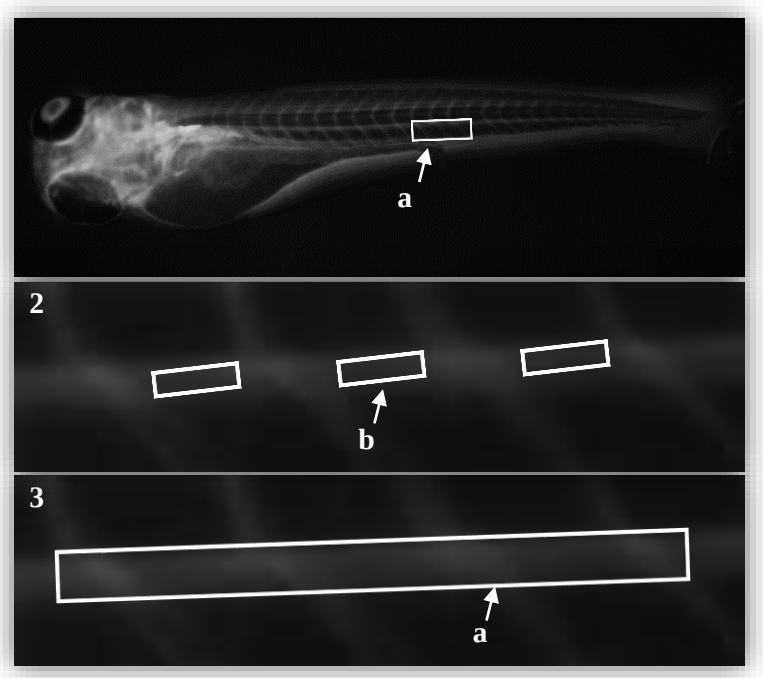

Figure 12 – FITC-intensity 2h after FITC-inulin injection. Zebrafish larvae (5 dpf) injected with 1.4 nL 2,5% FITC-inulin. **1-** Whole larvae; 2- Zoomed in image of the region over the caudal artery where the FITC-intensity was measured as in Rider *et al.* (2012); **3-** Zoomed in image of the region over the caudal artery where the FITC-intensity was measured; a - marked area shows the region in which the intensity value was acquired, covering the extent within the intersection of four intersegmental vessels and casing the three regions in which Rider *et al.* (2012) measures the FITC intensity. b - the three measurements performed by Rider *et al.* (2012).

Larvae with FITC-intensity values (mean grey value) under 50 were discarded, since the amount of injected FITC-inulin was so little that it could had run out before the 2h period. Also, larvae with fluorescence clots or injuries, resulting in extended damaged vessels, were discarded. The fluorescence measured 2h after injection was normalized with the fluorescence measured at 0h to correct for variability in initial FITC-intensity. Thus, results were expressed as percentage of FITC-intensity 2h after injection, which was calculated as the ratio – (FITC-intensity 2h / FITC-intensity 0h) *100.

Two replicates of the assay were performed for each drug and the minimal number of larvae that were injected for each drug in each replicate was 15 larvae. Control larvae were always injected in parallel with drug-exposed larvae, for comparison reasons and statistical analysis.

7. Transmission Electron Microscopy (TEM)

Nacre wt1b::GFP; cdh17::GFP larvae (4dpf) were exposed to the LC_{10} of each drug for 24h. After drug exposition, larva were euthanized with ice and fixed o/n in a fixation solution. Microwave procedure was used to fix the larvae (see annex II for a better explanation). After fixation, larvae were left in 100% EPON resin o/n. On the following day, molds were made with 100% resin at 60ºC in an oven.

Transversal sections were cut with a glass or diamond knife of 70 nm (for 2D micrograph), 100 nm (for serial sequences) or 120 nm (for tomograms), in the proximal convoluted tubules zone (when at least two parts of the tubule could be seen in the same side, since in this zone they are convoluted). For the serial images and tomograms, sections were sequentially cut. Sections were stained with 4x 1min uranyl acetate, 4x 1min water, 3min lead citrate and 5x 1 min water. For the tomograms, gold was added (10nm diameter) to the grids.

Photomicrographs were taken with a Transmission Electron Microscope (TEM, Hitachi H-7650). Three types of analyses were performed with TEM: 2D single micrographs, serial sequences and tomograms. 2D single micrographs are regular micrographs that were taken with a magnification of 1k, 3k, 5k and 10k per condition. Serial sequences consist on a z-series of 36 micrographs of the same cell (covering 360 nm of the cell, along the z-axis) from sequential sections, with a magnification of 3k; criteria for cell selection were that it was part of the tubules, fit wholly in the micrograph, nucleus was present and the apical side of cell ended in microvilli. For the tomograms, 111 micrographs were taken, with a magnification of 8k, on the same section, in the same spot, but with different angles (from -55^{o} to 55^{o}, with a 1^{o} increase); criteria for spot selection were a minimum of 3 mitochondria that fit in the same micrograph, mitochondria belonged in a cell from the tubule where the apical side ended in microvilli and in which the nucleus was present; 3 tomograms from 3 serial sections were performed for each condition.

Each set of 36 serial micrographs was opened with Fiji to set a scale and then saved as an image sequence. In a Linux environment (with the software Cygwin) they were converted to .st files and aligned with midas with the eTomo software. The aligned file was opened with the 3dmod software and a Z value, correspondent of the thickness of the section (19.85 pixels), was given to the micrographs.

Each tomogram was opened with Fiji and saved as an image sequence. In a Linux environment (with the software Cygwin) they were converted to .st files and aligned by tracking the gold beads with the eTomo software. The three sequential tomograms were then opened with eTomo, aligned with midas and saved as just one file.

The volumes of each object were obtained from the 3D models with the 3dmod software. Arbitrary units were attributed to the cells and mitochondria volumes; object volumes were normalized with either the respective cell, in 3D cell models, or with the respective mitochondrion, in 3D tomograms models. All volumes were displayed in bars graphics. To make the 3D models, both serial sequences and tomograms final files were opened with 3dmod and the contours of each object were manually drawn and meshed together. Movies were also made with 3dmod and saved as .avi files.

8. Statistical Analysis

Lethalities and FITC-intensities are expressed as mean and standard deviation. Larvae mortality is expressed as mean percentage.

Regarding the inulin assay, a t-test (IBM SPSS statistics v20) was applied in each experimental day ("intra-day" t-test) between the control (untreated larvae) and the drug-exposed larvae. A t-test ("inter-day" t-test) was applied between the 2 replicate experiments. Then, all results were joined per each condition and a one-way ANOVA test followed by Tukey HSD post-hoc test (IBM SPSS statistics v22) was performed among the 5 conditions. Correlations between urine and blood FITC-intensity were performed with pearson correlation coefficient. P-values < 0.05 were considered statistically significant. All parameters were expressed as means and standard deviation.

Results

1. *Lethality curves*

The lethality curves for TFV and its pro-drug, TDF, were traced, in *nacre wt1b*::GFP*; cdh17*::GFP zebrafish larvae, in order to understand the relationship between larvae death and the concentration of each drug.

Larvae exposed to higher drug concentrations (usually the 2 or 3 highest concentrations) experienced body curvature upwards/dorsal curvature (‘‘Cup’’ phenotype) and/or heart oedema with visible heart hemorrhage in some cases (Fig. 13.1). Swimming behavior was also reduced and the response to tail *stimuli* was retarded or absent when compared with control larvae. No alterations were observed in controls and larvae exposed to lower concentrations (usually the 2 lowest concentrations). Dead larvae presented i) no heartbeat with no necrosis at low or intermediate concentrations (Fig. 13.2) or ii) necrosis and body decomposition at the highest concentrations (Fig. 13.3).

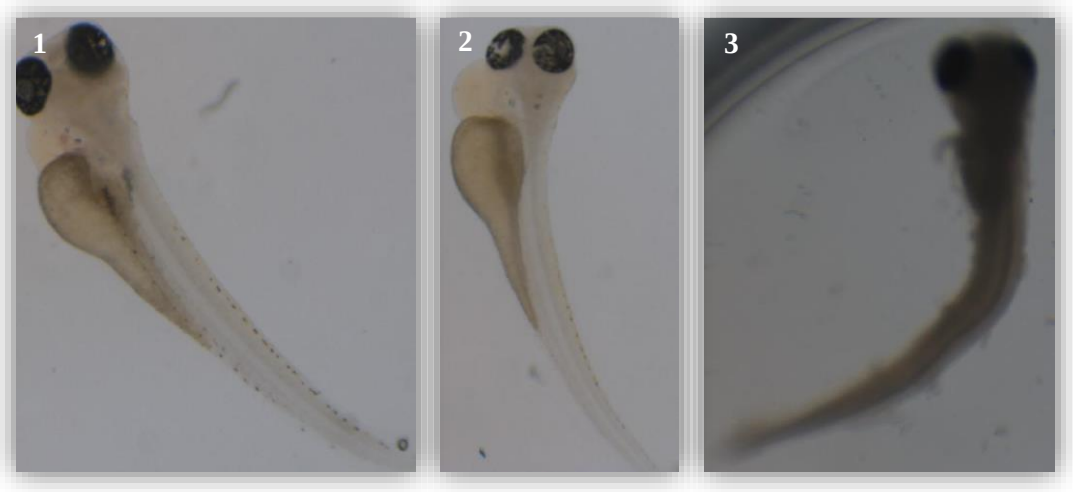

Figure 13 – Zebrafish larvae after 24h of TDF-exposition. (1) Zebrafish larvae with body curvature and heart oedema. (2) Dead zebrafish larvae with no necrosis. (3) Necrotic zebrafish larvae with body decomposition.

Lethality percentages for each drug (Annex III) were plotted against the logarithm of the drug concentration (Fig. 14.1). Lethalities were then transformed into probits for posterior LC_{10} calculations (Fig. 14.2), as in accord with Randhawa (2009) in his useful explanation of the “staircase method” for calculating LD_{50} from the method of Miller and Tainter, published in 1944, since this technique enables the linearization of experimental data (Randhawa, 2009; Randhawa and Arambasié, 2014).

1

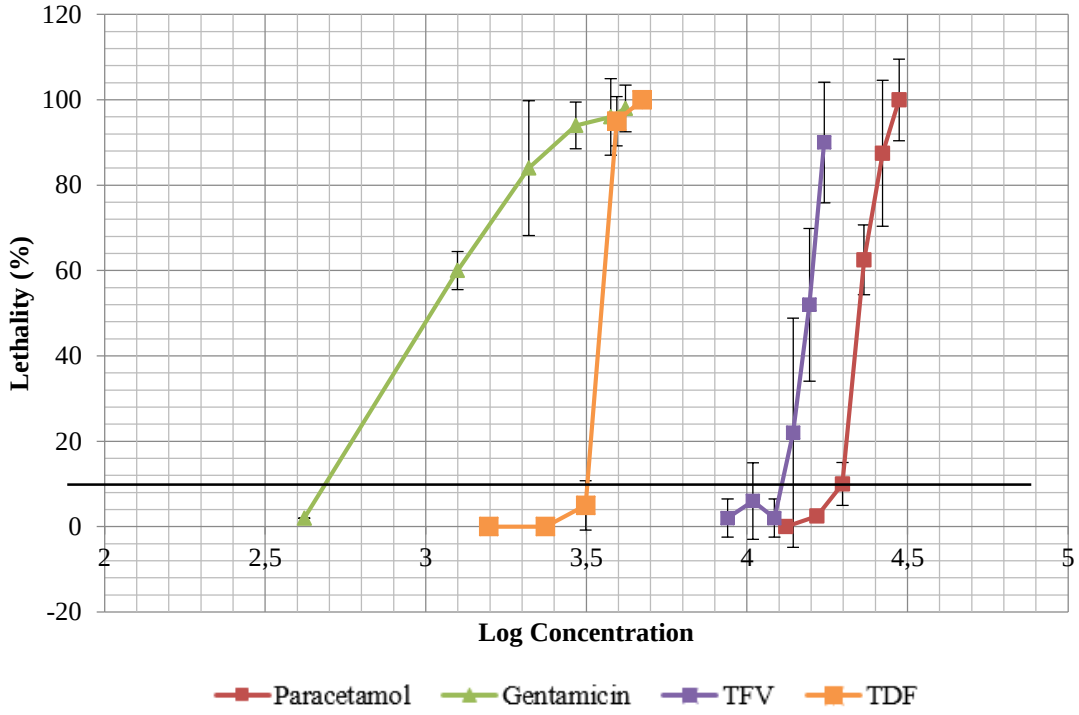

2

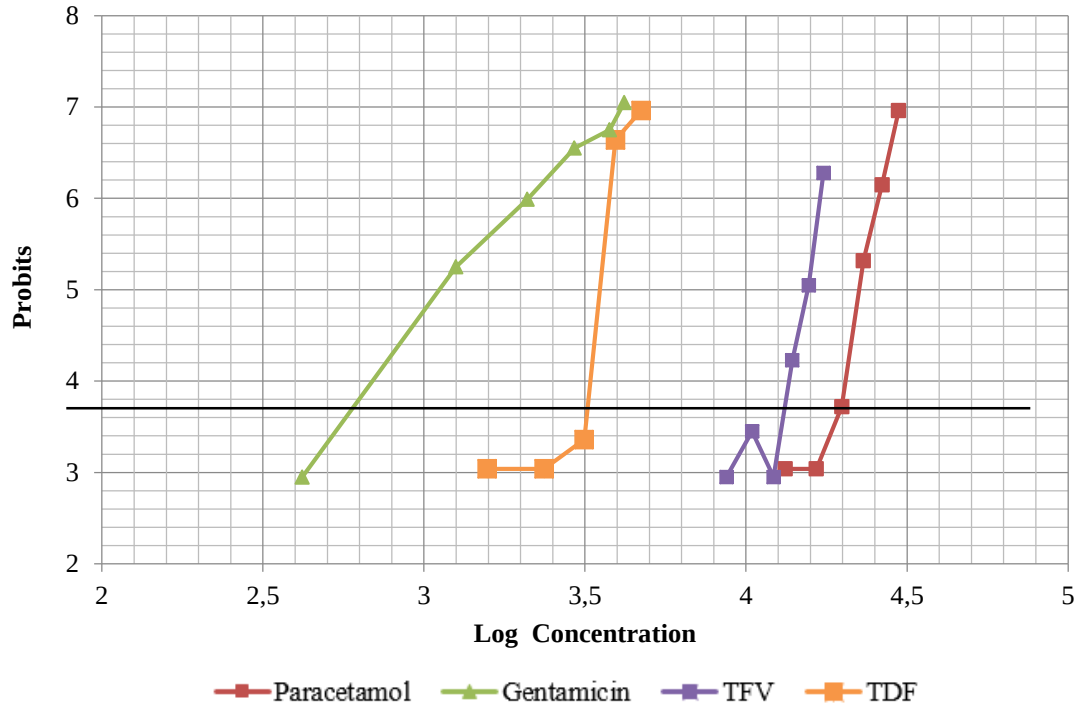

Figure 14 – Lethality curves for gentamicin, paracetamol, TFV and TDF. *Nacre wt1b*::GFP; *cdh17*::GFP larvae (4 dpf) were exposed to each drug by soaking for 24h. Lethality curves were obtained with 5 or 6 different concentrations (n=10 per concentration) in quadruplicate. (1) Lethality percentages were calculated for each drug, then mean and standard deviation were plotted against the logarithm of the drug concentration in µM; (2) Lehtalities were converted into probits, as stated by the Miller and Tainter method (Randhawa, 2009; Randhawa and Arambasié, 2014).

Regarding the left-right position of the curves, the order of the drugs (from the left to the right) was gentamicin, TDF, TFV and paracetamol (Fig. 14).

The slope of the curve and the LC_{10} and LC_{50} were calculated from the probit graphics. The results were summarized in the table 2, displayed below.

Table 2 – Slope, LC_{50} and LC_{10} values of each drug.

	Gentamicin	**Paracetamol**	**TFV**	**TDF**
Slope	4,0	12,1	10,4	9,0
LC_{50} (µM)	1243	21918	15334	3242
LC_{10} (µM)	596	17179	11541	2337

Gentamicin had the lowest slope value, 4.0, followed by TDF, TFV and paracetamol. TDF and TFV had very similar slope values, while gentamicin the most different (55.5 % lower than the second lowest value, TDF).

Also in accordance with the left-right position of the curves, the order of the LC_{10} and LC_{50} values, from the lowest to highest value was gentamicin, TDF, TFV and paracetamol. Interestingly, the TFV LC_{50} was 78.9% higher than the TDF LC_{50}.

2. Renal Function

In order to ascertain the glomerular function of drug-exposed larvae, a clearance assay was performed on *casper* larvae. Larvae of 4 dpf were exposed to the LC_{10} of gentamicin, paracetamol, TDF, TFV or the corresponding volume of water. 24h later, larvae were observed under the stereoscope and mortality rates were registered (Table 3).

Table 3 – Lethalities of the zebrafish larvae used for the FITC-inulin clearance assay. Zebrafish larvae were exposed to each drug or water (negative control) for 24h. The mean of the mortalities obtained in the two experiment replicates were registered in the table below. *volume of water correspondent to the volume of drug solution added to the EM.

	Control X µL water*	**Gentamicin** LC_{10}	**Paracetamol** LC_{10}	**TDF** LC_{10}	**TFV** LC_{10}
Mean Lethality %	0%	18.1%	11.2%	6.2%	1.3%

Alive larvae were then injected with FITC-Inulin in the CCV and FITC-intensity was captured by imaging laterally over the caudal region at 0h and 2h after injection (Ridder *et al*., 2012). Some larvae did not resist the FITC-injection and died in the 2h waiting period. The lethality rates are presented on the table 4.

Table 4 – Lethalities of the zebrafish larvae after FITC-inulin injection. *volume of water correspondent to the volume of drug solution added to the EM.

	Control X µL water*	**Gentamicin** LC_{10}	**Paracetamol** LC_{10}	**TDF** LC_{10}	**TFV** LC_{10}
Mean Lethality %	1.3%	30.6%	44.3%	2.8%	8.5%

A t-test was applied in each experimental day ("intra-day" t-test) between the control (untreated larvae) and the drug-exposed larvae. Those "intra-day" t-tests showed statistical differences only between controls and gentamicin and between controls and paracetamol. A t-test was applied between the 2 replicate experiments and showed no significant "inter-day" differences in each condition. Then, all results were joined per each condition and a one-way ANOVA test followed by Tukey HSD post-hoc test was performed among the 5 conditions.

The percentage of the FITC-intensity change after the 2h waiting period of the two joined replicate results can be seen in the figure 15. The ANOVA test was statistically significant ($p<0.001$) and verified the same differences that had already been seen with the t-tests. Post-hoc tests (Tukey HSD) revealed differences between controls and gentamicin ($p<0.001$) and controls and paracetamol ($p<0.001$).

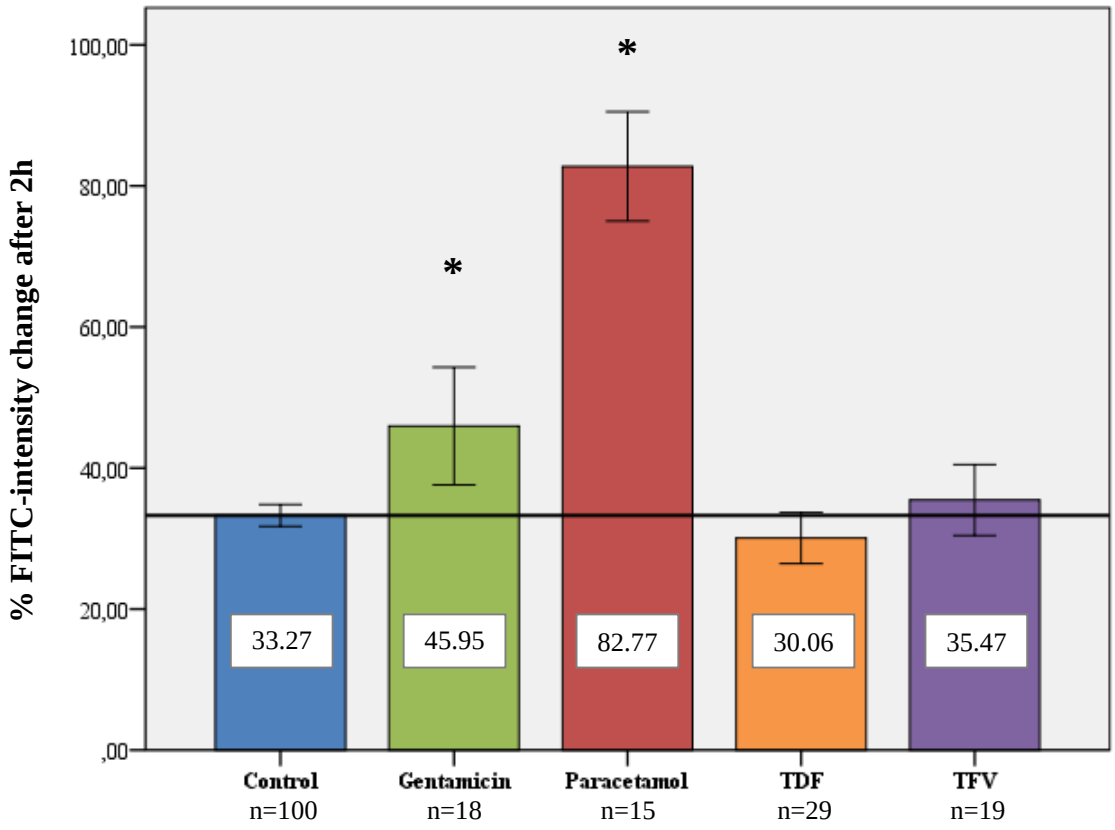

Figure 15 – Percentage (%) of FITC-intensity 2h after FITC-inulin injection. FITC-intensity values were measured at 0h and 2h after FITC-inulin injection and the 2h/0h FITC-intensity ratios were calculated. White boxes represent the mean value and the bars represent the standard deviation for each condition of the 2 replicates. One-way ANOVA followed by Tukey HSD hoc-test/post-test demonstrated differences statistically significant between control and gentamicin or paracetamol. The n of each condition is presented under it. * $p<0.001$.

In this assay, gentamicin or paracetamol -exposed larvae had significantly higher FITC-intensity percentage values (both p-value < 0.001) 2h after FITC-inulin injection than controls. While control larvae experienced a drop in FITC-intensity from 100% (values were normalized) to 33.27 ± 7.90%, gentamicin-exposed larvae FITC-intensity only reached 45.95 ± 16.78%, a 27.60% higher value than controls (Fig. 15). Paracetamol-exposed larvae retained an even higher FITC percentage, 82.77 ± 13.97%, which were 59.80% more than control larvae (Fig. 15). Contrariwise, TDF or TFV -exposed larvae FITC-intensity values were not significantly different when compared to controls (both p-values > 0.05), 30.06 ± 9.50% and 35.47% ± 10.42% respectively (Fig. 15).

Gentamicin -exposed larvae FITC-intensity was significantly different from TDF or TFV -exposed larvae FITC-intensity ($p<0.05$ and $p<0.001$, respectively); paracetamol -exposed larvae FITC-intensity was also significantly different from TDF or TFV -exposed larvae FITC-intensity (both $p<0.001$); gentamicin or paracetamol -exposed larvae FITC-intensity was significantly different between each other as well ($p<0.001$). No differences in FITC-intensity were found between TFV or TDF -exposed larvae ($p>0.05$).

3. *Transmission Electron Microscopy*

In order to identify mitochondrial ultrastructural changes happening in the inside of cells from the convoluted tubules of drug-exposed zebrafish larvae, ultrathin sections of the convoluted tubules zone were cut so that they could be analyzed by TEM. 10 *nacre wt1b*::GFP*; cdh17*::GFP larvae of 4 dpf were exposed to the LC_{10} of gentamicin, paracetamol, TDF, TFV or water. The lethalities obtained in each condition were summarized in the table 5. All organelles were observed and compared within the different conditions, but mitochondria were more minutely studied.

Table 5 – Larvae lethalities percentage for the TEM experiments.

Exposition	**Control** **X µL water***	**Gentamicin** **LC_{10}**	**Paracetamol** **LC_{10}**	**TDF** **LC_{10}**	**TFV** **LC_{10}**
Lethality	0%	16.67%	0%	0%	0%

a. 2D micrographs

On a first analysis, simple 2D micrographs, from one larvae per condition, were taken on 70 nm sections, with a 1k, 3k, 5k and 10k magnification. Micrographs from the drug-exposed larvae were visually compared to the ones from control larvae (figures 16). 1 to 3 sections per condition were analyzed and all portions of the tubule captured by the micrographs were screened. That totaled a minimum of 50 cells per condition.

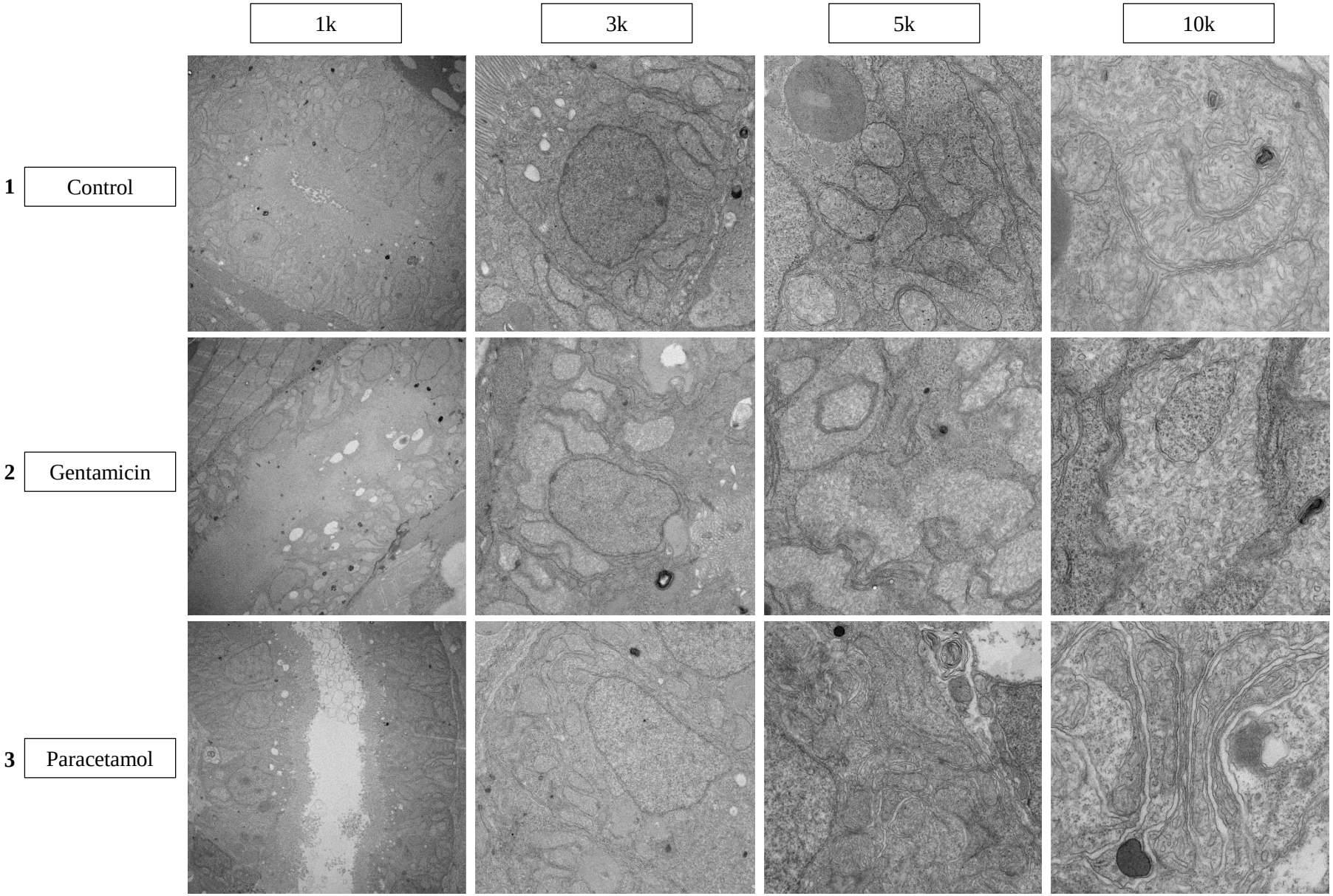
1k
3k
5k
10k
1
Control
2
Gentamicin
3
Paracetamol

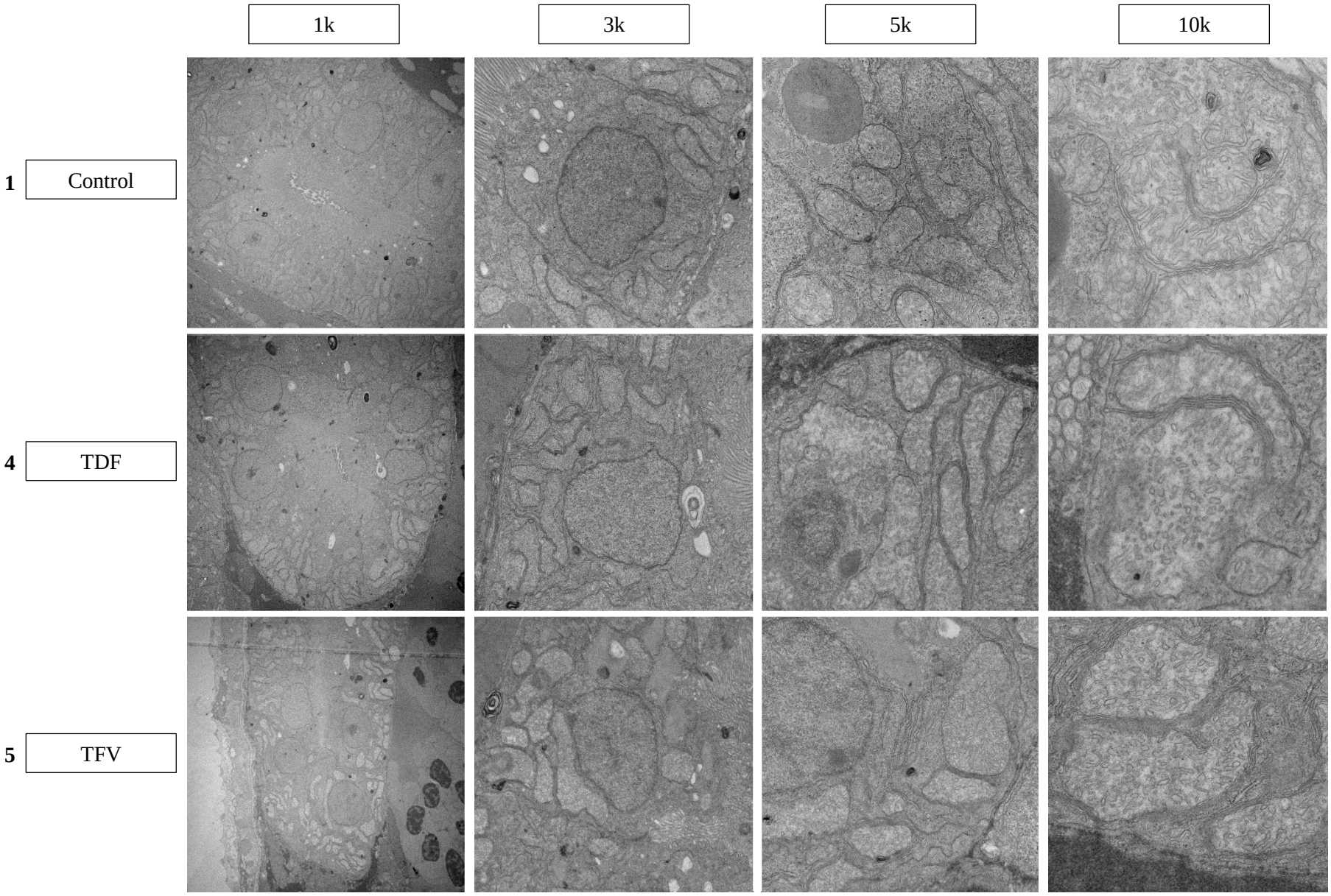
1k
3k
5k
10k
1
Control
4
TDF
5
TFV

Figure 16 – 2D micrographs of convoluted tubules from zebrafish larvae. The micrographs belong to one larvae per condition and were obtained by TEM. The amplification of each micrograph (1k, 3k, 5k or 10k) is placed above it. (1) Micrographs from a control larvae. (2) Micrographs from a gentamicin-exposed larvae. (3) Micrographs from a paracetamol-exposed larvae. (4) Micrographs from a TDF-exposed larvae. (5) Micrographs from a TFV-exposed larvae.

With the 1k magnification it was possible to observe the contours of the tubule, as well as the cells that comprise it, and have a general idea on their appearance. The tubule, independently of the condition, was usually composed of one cell layer, with the basal membrane leading to the outside of the tubule and the apical membrane ending in microvilli[9] that gave in to the lumen of the tubule (Fig. 16, 1k micrographs). When present in the lumen, cilia could also be seen (Fig. 17). Exceptionally, higher magnification micrographs (20k) were taken to better show the cilia structure (Fig. 17.2).

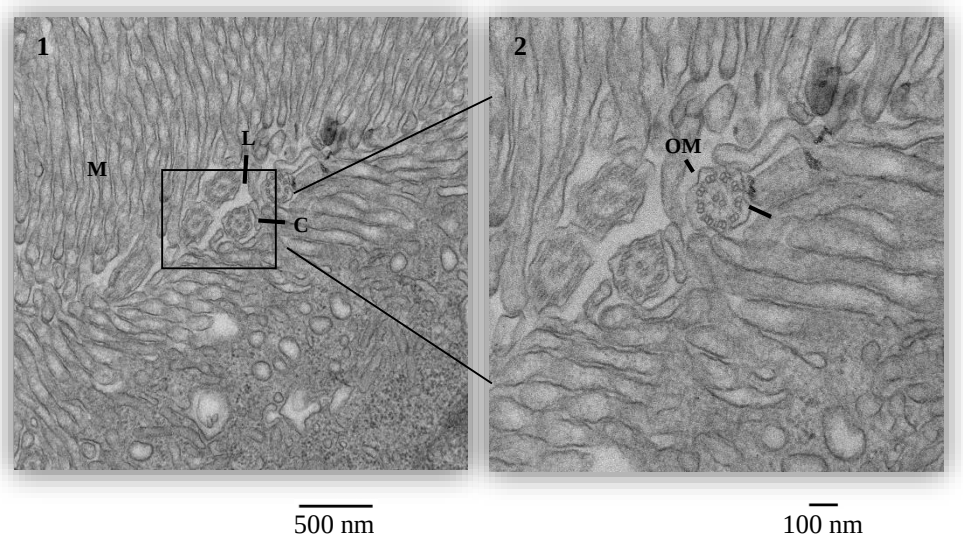

Figure 17 – Transversal section of cilia present in the lumen of the convoluted tubules of a zebrafish larvae after TFV exposition. (1) 3k micrograph from the lumen of a tubule containing 4 cilia; microvilli can also be seen in the lumen and surrounding the cilia. (2) 20k micrograph of the previous figure, showing a well-focused cilia; the outer membrane can be seen, as well as the central singlet microtubules (in the middle of the cilia) and the 9 peripheral doublets microtubules (Fawcet, 1981). L- lumen; M – microvilli; C – cilia; OM – outer membrane; MD – peripheral doublet microtubule.

With the 3k magnification it was possible to observe a whole single cell, in most cases (Fig. 16, 3k micrographs). Cells usually displayed a rectangular or square shape, with the nucleus in the center and the mitochondria in the basal and lateral sides, although it was also observed, albeit rarely, the presence of some mitochondria in the apical side. This pattern was observed in all conditions. The nucleus had a round shape and was delimited by a membrane. It was possible to distinguish the heterochromatin from the euchromatin, as the first acquired a darker color. Nucleolus was also captured in some cell's nucleus. Mitochondria were bounded by an inner and an outer membrane and were characterized by having inner membrane invaginations, the cristae, which projected into their interior. Other organelles, *i.e.* the rough

[9] Extensions of the cell membrane.

and smooth endoplasmic reticulum (RER and SER, respectively), Golgi apparatus, lipids and membrane deposits, lysosomes and/or peroxisomes could also be seen (Fig. 18). The RER was identified by presenting elongated or circular membrane-bounded channels, parallel to each other, with several ribosomes, tiny black dots, attached to it (Fig. 18.3). It was not possible to distinguish the SER form the Golgi apparatus, as both have a similar morphological appearance (Fig. 18.3). The Golgi apparatus and SER shape is similar to the RER, with the exception of the adherent ribosomes not being present. Lipid deposits appeared as dark circles that were not membrane bounded (Fig. 18.1). Membrane deposits were identified by showing several dark rings tightly packed (Fig. 18.2). Grey circular, oval or elliptical structures were also present in some cells and were identified as either being lysosomes or peroxisomes (Fig. 18.4). Since it is not possible to positively identify them with morphological criteria alone, a histochemical demonstration of one or more of their constituent enzymes would have to be performed (Fawcet, 1981).

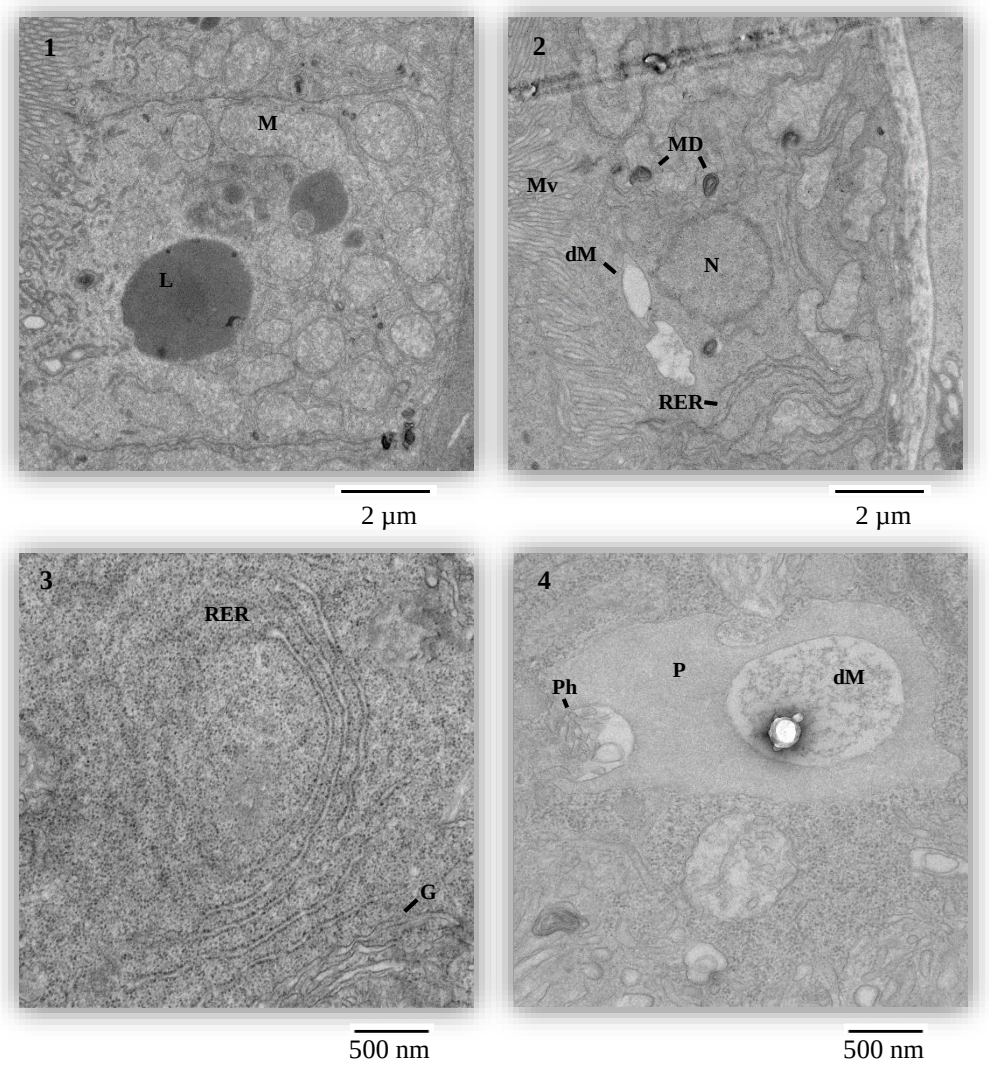

Figure 18 – Transversal sections of the convoluted tubules after water or drug exposition showing several cell structures. (1) 3k micrograph of a cell from a control larvae, showing 2 lipid deposits and several mitochondria. (2) 3k micrograph of a cell from a TFV-exposed larvae, showing the nucleus, microvilli, mitochondria, membrane deposits, 2 damaged mitochondria and the RER. (3) 10k micrograph of a paracetamol-exposed larvae, showing the RER and what appears to be the Golgi apparatus or the SER. (4) 10k micrograph of a TFV-exposed larvae, showing what appears to be a peroxisome or a lysosome phagocyting a damaged mitochondria. L – lipid deposit; M – mitochondria; Mv – microvilli; nM – damaged mitochondria; MD – membrane deposits; N – nucleus; RER – rough endoplasmic reticulum; G – Golgi apparatus or SER; Ph – phagocytosis; P – peroxisome or lysosome.

Even though mitochondria and the other organelles and cell structures were quite visible and evident in each 3k micrograph, the 5k magnification enabled to see them with even more detail (Fig. 16, 5k micrographs). It was possible to denote differences in mitochondria shape, color (in a grey scale; lighter or darker) and matrix granules content.

The cristae ultrastructure of each mitochondria was observed with the 10k magnification, as well as the matrix granules when their nature was dubious in the 5k micrographs (Fig. 16, 10k micrographs). With this magnification, it was also possible to see free ribosomes – tiny black dots distributed through the cytosol. The membranes of all organelles – cilia, nucleus, mitochondria, cell membrane, RER, SER – were a little wavy in all conditions.

Control larvae (Fig. 16.1) showed, in general, round or roundish shaped mitochondria, with smooth contours and regular shapes, although different in size. They did not gathered in any apparent clusters, rather they were equally spaced. The cristae showed as thin, long cylindrical shapes, distributed along the mitochondria in different orientations, and the matrix granules occurred outside the cristae as tiny black dots. Some matrix granules appeared lobulated.

Albeit not every mitochondria from paracetamol-exposed larvae appeared altered, some looked smaller and thinner, and gave the impression of forming clusters of several small mitochondria (Fig. 16.2). Other mitochondria showed long and thin. They also showed a reduction in the number of matrix granules and a small part of the cristae seemed degraded, since they occurred circular and scattered instead of cylindrical.

Gentamicin-exposed larvae (Fig. 16.3) showed enormous and light mitochondria with very irregular shapes and contours with sharp angles. The cristae appeared mostly degraded and very scattered, with several empty spaces between them. Mitochondria did not had any matrix granules.

TFV and TDF -exposed larvae mitochondria phenotype was similar to that found in gentamicin-exposed larvae, albeit not as pronounced – mitochondria were not as large and a higher portion of normal mitochondria were encountered there than in the gentamicin-exposed larvae; cristae looked degraded, but also not as extensively as in gentamicin-exposed larvae cristae. Still, none had matrix granules.

The RER, SER and/or Golgi apparatus, membrane and lipid deposits, lysosomes and/or peroxisomes were present in all conditions; comparisons on their shape and appearance are discussed in the discussion of this thesis.

b. 3D models of serial sequences

Because the 2D micrographs cannot offer an accurate perspective on mitochondria volume and shape, a z-series of 36 successive micrographs were taken and aligned together. A depth "Z" was attributed to each micrograph and the contours of each cell structure or object – cell membrane, mitochondria, lipids and membrane deposits, lysosomes or peroxisomes and nucleus – were manually drawn and meshed together to create a 3D model of one cell. Only a portion of the cell was represented in the 3D models (360 nm, along the z-axis), in the area correspondent to approximately half of the nucleus, in both models. The full videos can be seen in the CD-ROM.

So far, only 3D models of cells from control and TFV-exposed larvae were finished, and they can be seen on the figures 19.

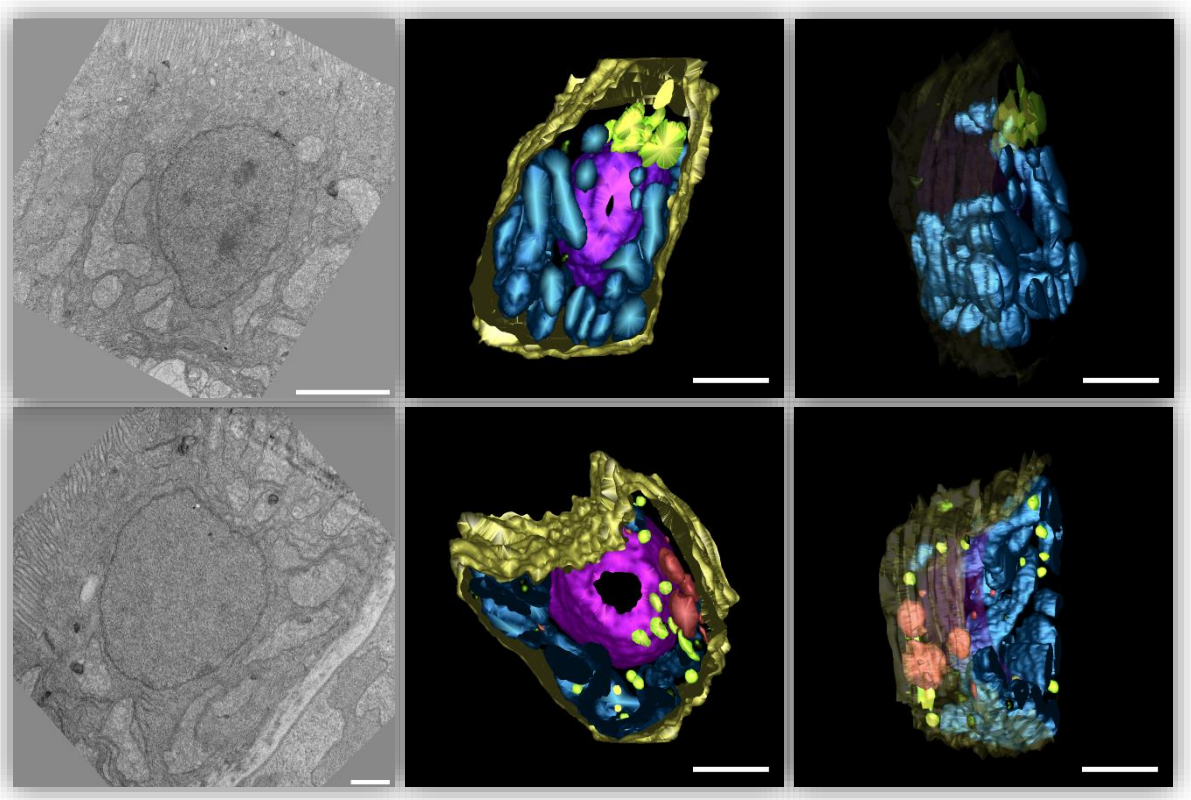

Figure 19 – Snaps of the serial sequences 3D cell models. 3D cell models were constructed after the alignment of 36 serial micrographs with a 3k magnification of the same cell. Left image represents one of the micrographs taken of the cell; middle image is the front view of the cell; right image represents a side view of cell, with cell membrane and nucleus translucent for a better view of the mitochondria. (1) Control larvae cell. (2) TFV-exposed larvae cell. Yellow – cell membrane; purple – nucleus; blue – mitochondria; light green – lysosomes and/or peroxisomes; dark green – membrane deposits; red – damaged mitochondria. Scales bar: 2520 nm

The cell from the control larvae had a rectangular shape that was maintained throughout its length, with the apical side, were the microvilli start, on the top of the snap (Fig. 19.1, left and middle). The nucleus had a half-sphere profile that was also maintained throughout the length of the model. Mitochondria occurred on the basal and lateral sides, in varied shapes and sizes. It was possible to observe that most mitochondria were interconnected with each other, forming a vast mitochondria network, so that only a small portion was individually separated from the rest (Fig. 19.1, right). Although mitochondria shape varied greatly, they generally had thin roundish forms. Lysosomes and/or peroxisomes were present in the apical side, with circular or elliptical shapes. Several membrane deposits were scattered in the cytosol.

The cell from the TFV-exposed larvae had a rectangular shape, with the apical side on top left corner (Fig. 19.2, left) or top right corner (Fig. 19.2, middle), albeit the left side had a half-moon contour. The nucleus also had a half-sphere shape and the mitochondria were scattered through the basal and lateral sides of the cell. Mitochondria assumed large roundish shapes and, in semblance with those from the controls, formed bridges between each other, albeit the network was not as extended, *i.e*. mitochondria did not form as many connections with each other (Fig. 19.2, right). Several small lysosomes and/or peroxisomes occurred scattered in the cell, as well as membrane deposits. Also, several white spots occurred in the apical side, which appeared to be autophagosomes eliminating damaged mitochondria, as what appeared to be cristae remains were seen in its inside (Fig. 20).

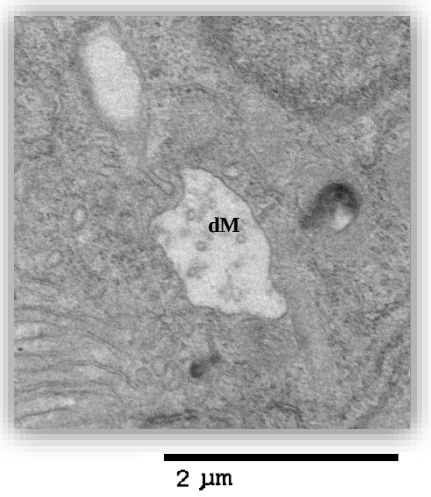

Figure 20 – Damaged mitochondria. Zoomed in image of one micrograph (3k magnification) from the 36 z-series of the TFV-exposed larvae cell showing two damaged mitochondria.

Through the created models it was possible to calculate the volume of each object, *i.e.* each cell structure whose contours were traced. Figure 21.1 shows the cells volume; arbitrary units were attributed to the

cells volume. Figure 21.2 shows the nucleus and mitochondria respective volumes while figure 21.3 shows the lysosomes and/or peroxisomes, membrane deposits and damaged mitochondria volumes.

1

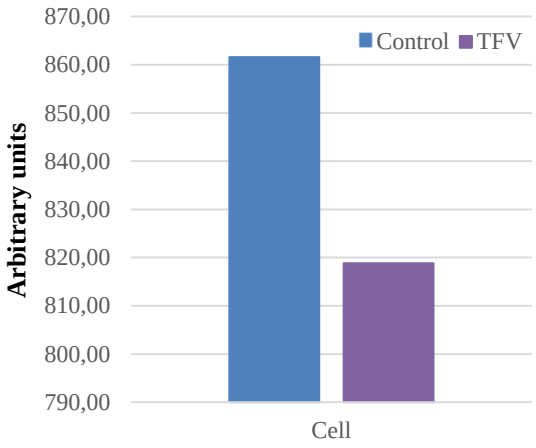

2

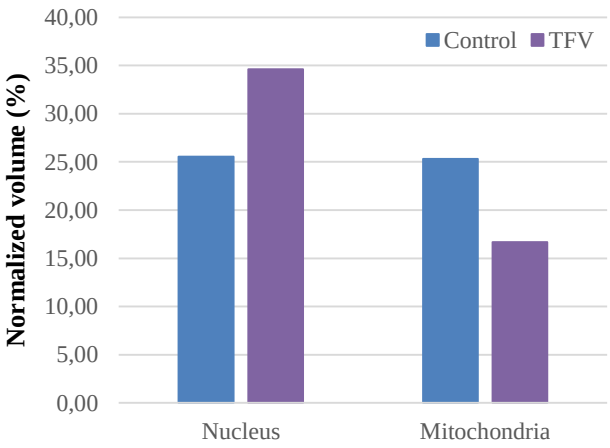

3

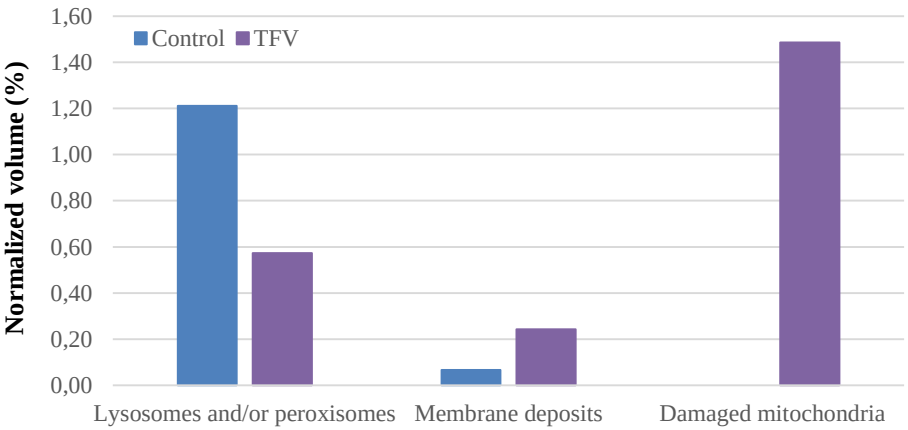

4

	Control	TFV
Cell *	861.62	818.84
Nucleus	25.55%	34.62%
Mitochondria	25.33%	16.67%
Lysosomes and/or peroxisomes	1.21%	0.57%
Membrane deposits	0.07%	0.24%
Damaged mitochondria	0.00%	1.49%

*Arbitrary units

Figure 21 – Volumes of the organelles obtained with the 3D cells models. (1) Control and TFV-exposed larvae cell volume in arbitrary units. (2) Nucleus and mitochondria volumes, normalized with the cell volume. (3) Lysosomes and/or peroxisomes, membrane deposits and autophagosomes with damaged mitochondria volumes normalized with the cell volume. (4) Summarized volumes of each object.

The cell volume of the control larvae was 4.97% higher than TFV-exposed larvae. The nucleus in TFV-exposed larvae had a higher volume than the control larvae cell nucleus, approximately 26.20% higher. Mitochondria occupied 25.55% of the total cell volume of the control cell, 37.19% more than TFV-exposed larvae. Lysosomes and/or peroxisomes from control larvae also occupied a higher volume, 52.89%, contrary to the membranes deposits which volume was 70.83% higher in the TFV-exposed larvae cell. Damaged mitochondria totalized 1.49% of the total TFV-exposed larvae cell volume.

c. 3D models of tomograms

The 2D micrographs could not give an accurate perspective on cristae shape, since they can only offer a 2D perspective. The 3D models of serial sequences also could not offer a good view on cristae shape, as they i) had a too low magnification (cristae did not show with a high resolution) and ii) they had "jumps" among micrographs. These "jumps" (Fig. 22.1), even though they are not perceptible for bigger structures, such as the nucleus and mitochondria, appear because the section from where the micrographs are taken have a 100 nm depth, which is thick enough to show dramatically changes in smaller structures, such as the cristae, from one micrograph to the next one. In contrast, tomograms take z-series of micrographs on the same section from several different angles (Fig. 22.2) and thus can give a 3D perspective of the whole section, enabling us to follow the cristae morphology.

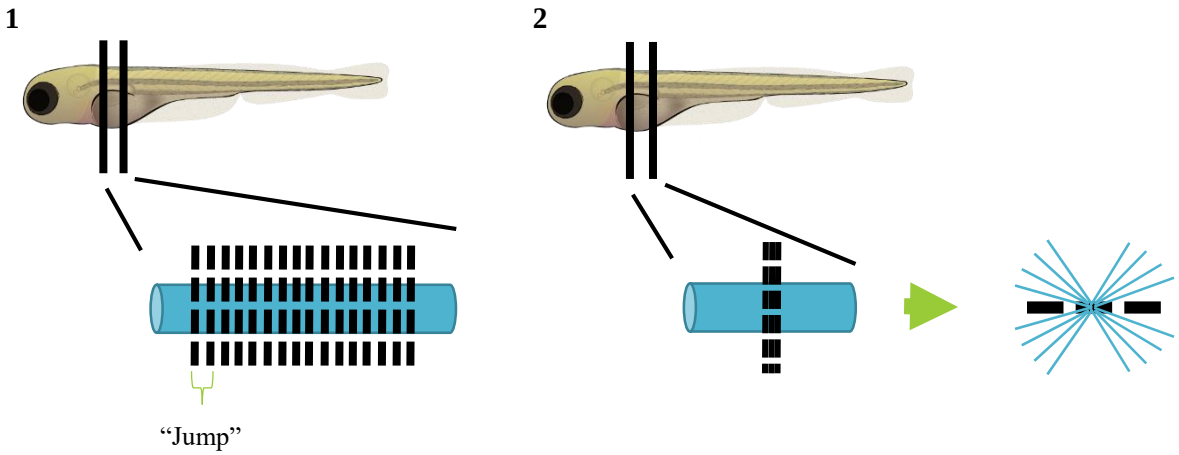

Figure 22 – Scheme of how serial sequences and tomograms were performed. (1) A z-series of 36 micrographs in total was taken on different, sequential, sections; the image also illustrates the "jumps" that occur from one micrograph to the next one. (2) A tomogram analysis was performed on each section (3 in total); each tomogram was made by taking a micrograph from several different angles (from -55º to +55º), performing a total of 111 micrographs, which were later joined to create a 3D image perspective of the whole section. *Zebrafish larvae illustration adapted from Lizzy Griffiths (in http://zebrafishart.blogspot.pt).*

Therefore, 3D models of a portion of a mitochondrion were made by tomography. The mitochondria membrane, cristae and matrix granules were delineated manually to create a 3D structure that represented a portion of a mitochondrion. So far, only one model from one mitochondrion from the controls and one from TFV-exposed larvae was finished and they can be seen on the figure 23.

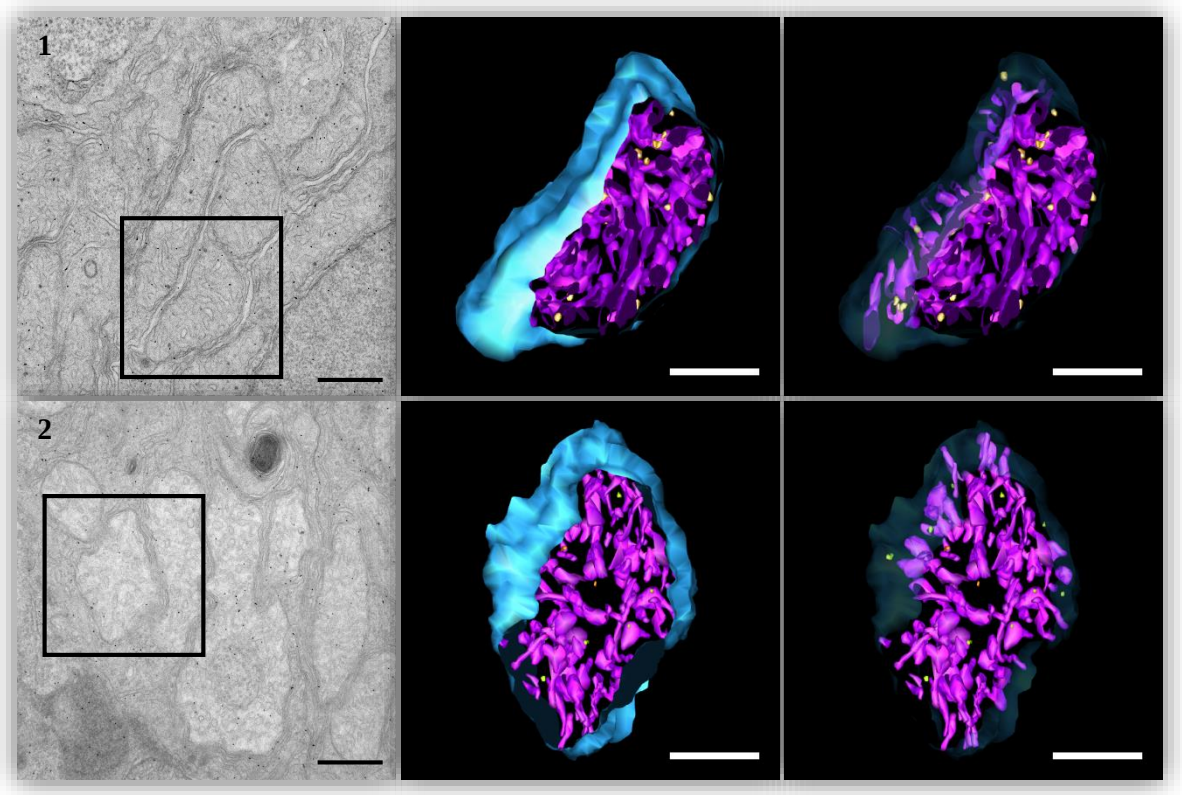

Figure 23 – Snaps of the 3D tomograms models. Left image represents the micrograph at 0º taken from the tomogram analysis; middle image the model view of the mitochondrion; right image represents the mitochondrion with its membrane translucent for a better view of the cristae, matrix granules and cristae remains when present. (1) Control larvae mitochondrion. (2) TFV-exposed larvae mitochondrion.Blue – mitochondrion membrane; magenta – cristae; orange – matrix granules; green – cristae remains. Scales bar: right left image – 500 nm; middle and right images – 284 nm.

Only a portion of the mitochondrion was captured in each joined tomogram. The full videos can be seen in the attached CD-ROM.

The 3D tomogram model showed that the mitochondrion from the control larvae had an oval shape and densely packed cristae with several round matrix granules (Fig. 23.1). It was possible to see the places where mitochondrion invagination took place to form cristae. Cristae branched from several places, creating bridges that interconnected with each other and forming a dense network. Matrix granules intercalated freely in the mitochondrial matrix, without any apparent pattern (Fig. 23.1, right image).

The 3D tomogram model from the TFV-exposed larvae showed that the mitochondrion was also oval shaped but, opposite to the control, cristae were clearly disrupted and there was a marked loss of matrix granules (Fig. 23.2). Cristae branching was not as present as compared to what was seen in the control,

rather most cristae stood as short unbranched membrane invaginations and some even appeared to be isolated and unconnected to the inner membrane. Also, structures that resembled small spheres and that were not identified through the micrographs were revealed by the tomograms. These structures were of the same size as matrix granules but differentiated from them by having an empty interior, giving the impression that they were cristae remains originated from cristae fragmentation.

The volume of the mitochondrion and the normalized volumes of the cristae, matrix granules and cristae remains are displayed in the bars graphics below (Fig. 24).

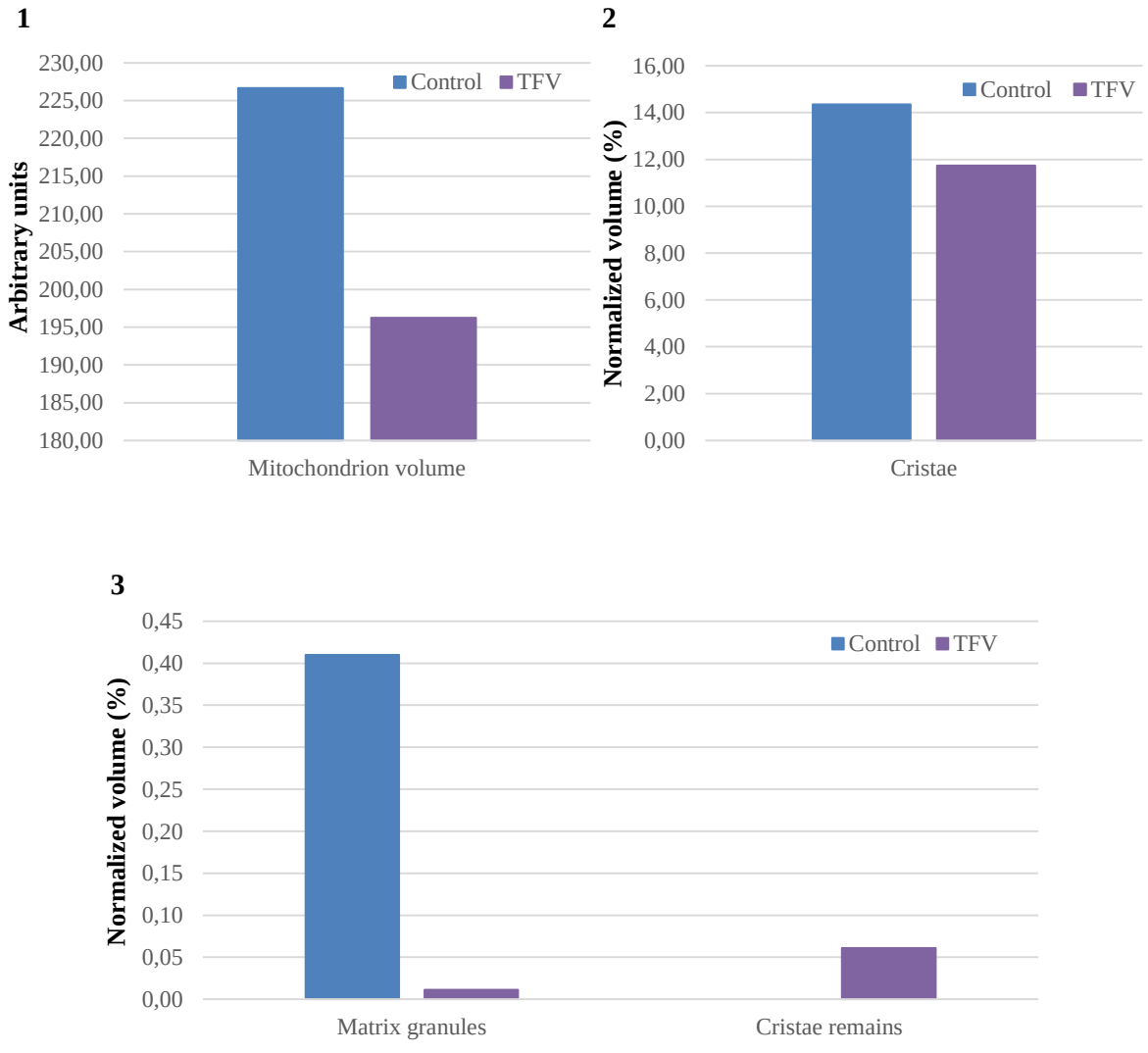

4

	Control	TFV
Mitochondrion *	226.66	196.25
Cristae	14.35 %	11.74 %
Matrix granules	0.41 %	0.01 %
Cristae remains	0.00 %	0.06 %

*Arbitrary units

Figure 24 – Volumes of the 3D tomograms models. (1) Control and TFV-exposed larvae mitochondrion volume; values were displayed in arbitrary units. (2) Cristae volumes normalized by the mitochondrion volume. (3) Matrix granules and mitochondria remains volumes normalized by the mitochondrion volume. (4) Summarized volumes of each object

The mitochondrion volume from the control larvae was approximately 13.42% higher than the one from the TFV-exposed larvae (226.66 opposed to 196.25, respectively; arbitrary units). The cristae, matrix granules and cristae remains total volume were normalized to the respective mitochondrion volume. Cristae occupied 14.35% of the control respective mitochondrion volume, approximately 18.19% more than the TFV-exposed larvae mitochondrion, while matrix granules occupied 0.41% of the mitochondrion volume, approximately 97.56% more than in the mitochondrion from the TFV-exposed larvae. Cristae remains totalized 0.06% of the TFV-exposed larvae volume.

Discussion

For this thesis, acute toxicity was induced in zebrafish larvae by tenofovir, as well as by two other nephrotoxicity drugs, gentamicin and paracetamol, that were used as positive controls. For all these drugs, lethality curves, GFR and ultrastructural tubular alterations were evaluated.

Before discussing the results obtained through the course of this thesis, some general limitations over the whole work will be discussed.

Tenofovir is administrated to HIV patients chronically, so its toxic effects are mostly associated with a chronic exposition rather than an acute one. Because this was a first trial and it was not guaranteed that the larvae would report any differences, an acute toxicity assay was chosen to be performed instead of a chronic one, in order to reduce the workload.

On every experiment performed in this thesis, environmental factors, such as temperature, water pH, properties and composition of the EM, were, in principle, all controlled and equal between experiments and replicates. Genetic factors were also controlled, since the zebrafish were inbreed animals[10], so in principle genetic variations between the larvae were not present. However, even thought environmental and genetic factors were kept constant among experiments, zebrafish larvae did not always respond in the same way to the toxic insult. All experiments were performed with a LC_{10} drug concentration, but a 10% mortality was not observed in every experiment (see table 3 and 5).

This could have been due to differences in drug absorption, since it is a factor that could not be fully controlled. In larvae of 4 dpf, drug absorption is done mainly through the skin and in some extent by the gills since drug delivery was performed by soaking. Some variations in larvae mortality, possibly caused by different amounts of drug absorption, are expected to occur (Kumar *et al*., 2013; Chaudhari *et al*., 2013).

One of the aims of this thesis was to measure the mitochondrial DNA of zebrafish larvae when exposed to tenofovir, since several studies performed in humans and other animal models, reported a decrease in the mitochondrial DNA. This analysis would give a more accurate quantification of the mitochondrial population, since it would be possible to measure the mitochondrial DNA relative to the genomic DNA, thus controlling for the number of cells. And since one of the zebrafish lines that was used expressed GFP in the pronephros, FACS (Fluorescence-Activated Cell Sorting) could be used to select the cells from the pronephros, as well as the gut cells and other fluorescent cells in order to quantify specifically

[10] Strains that are essentially homozygous for all loci (homozygous in 98.4% of their genes). These animals have a known genetic profile and are phenotypically, metabolically and physiologically homogenous, i.e., they are not diverse, unlike natural population (Nóvoa, 2014)

the mitochondria from the pronephros. Unfortunately, although FACS was performed on drug-exposed *nacre wt1b*::GFP*; cdh17*::GFP larvae, qPCRs were not totally optimized for time limitation reasons (some problems appeared with the mitochondrial primers). For that reason, the results were excluded but the protocols used can be seen in the annex IV.

1. Lethality curves

The position of the lethality curve along the log concentration is related with the toxic potency of the drug. A drug whose curve is on the right side would need lower concentrations than a drug whose curve is on the left side to kill the same percentage of the population. This order is intimately related to LC_{10} and LC_{50} values, since lower values translate into a more left-side position of the curve and higher values into a more right-side position (Stark and Banks, 2003).

In this case, gentamicin was the most powerful drug in terms of lethality, since it was the first to appear on the left, followed by TDF and TFV and lastly, paracetamol, the less toxic since it appears on the right side (Fig. 14). The LC_{10} and LC_{50} values were in accord with the left-right position of the curves, as it was to be expected, since lower values translate into a higher toxic potency: gentamicin had lower LC_{10} and LC_{50} values, followed by TDF, TFV and paracetamol (Table 2).

Regarding the shapes of the lethality curves, all drugs exhibited sigmoidal curves but with different slopes (Fig. 14). Gentamicin had the shallowest slope and, consequently, the lowest slope value, followed by TDF, TFV and paracetamol, which had the steepest slope and the highest slope value.

The slope of the curve is related with the mechanism of drug toxicity. While paracetamol, TDF and TFV had relatively similar slope values (12.1, 10.4 and 9.0, respectively), gentamicin had the most different, only 4.0 (Table 2). This could mean that gentamicin has a very different mechanism of drug toxicity. TFV and TDF have similar slope values, which could probably mean that they have a similar mechanism of drug toxicity, possibly because the same molecule is responsible for the toxicity. As it is, the only difference between TDF and TFV registered by the lethality curves was in their bioavailability[11], which translates into different LC_{10} and LC_{50} values. Because TDF is more bioavailable than TFV, LC_{50} and LC_{10} values are lower for TDF than TFV.

It can be speculated why it is needed to expose the larvae to higher drug concentrations of TFV than TDF. As it was explained earlier, drug absorption is mainly done through the skin. Membranes are negatively charged and thus the ionic state of the drugs limits its absorption. Unlike TFV, in TDF the two negative charges are masked by two isopropyloxycarbonyloxymethyl moieties, turning the

[11] Measurement of the rate and extent to which a drug reaches the site of action.

molecule into a non-ionic state, and therefore more permeable across the membranes (Gelder *et al*., 2002; Geboers *et al*.). As it is, TDF is absorbed more easily than TFV, which means that TDF has higher bioavailability than TFV. Larvae are probably able to absorb higher concentrations of TDF than TFV, and that might account for the higher lethality power of TDF.

2. Renal Function

GFR is a quantitative measure of renal function, *i.e.* the capacity of the glomerulus to filter the blood. GFR can be easily measured by injecting inulin into the blood stream, since inulin is completely filtered at the glomerulus but neither reabsorbed nor secreted in the tubules. Renal clearance or GFR can be calculated by measuring the plasma or urine concentration of inulin before and after a specific period of time, assuming that the overall volume of distribution is constant and the kidney is the only path of excretion (Hentschel *et al*., 2004). In this case, inulin was attached to the green fluorophore FITC so that inulin changes could be easily measured by assessing the FITC-intensity in the blood. So, high blood FITC-intensity values, when compared with controls, would mean that there was a retention of inulin in the blood and thus, that the glomeruli filtration function was decreased.

In this assay, both gentamicin-exposed larvae and paracetamol-exposed larvae had a significantly higher percentage of remaining FITC-intensity in the blood stream when compared with controls ($\%FITC_{Control} = 33.27 \pm 7.90$; $\%FITC_{Gentamicin} = 45.95 \pm 16.78$, $p<0.001$; $\%FITC_{Paracetamol} = 82.77 \pm 13.97$; $p<0.001$), meaning both effectively decreased the glomerular function. Albeit paracetamol induced bigger alterations in the renal function, gentamicin might be considered as a more sensitive control, as the reduction in renal function was milder.

Hentschel *et al.* (2004) injected 50–54 hpf (hours post fertilization) zebrafish larvae with gentamicin and at 72 hpf with FITC-inulin. They observed a 75% reduction in the renal function, 24h after, in the gentamicin injected larvae in relation with the controls. Rider *et. al.* (2012) observed a 17.5% reduction of the renal function, 4h after injecting 72 hpf larvae with gentamicin and at 100 hpf with FITC-inulin. As far as we know, renal function in paracetamol-exposed larvae has never been measured. But, Peng *et al.* (2010) reported mild to severe morphological changes in the glomerulus after exposing zebrafish larvae from 12-60 hpf to different concentrations of paracetamol. Therefore, both gentamicin and paracetamol were accounted as positive controls for renal function measurement.

Neither TDF nor TFV reduced renal function in larvae, as the ANOVA test did not indicate any difference in relation to the negative control. As far as we know, there are no reports of renal function measured in tenofovir-exposed zebrafish, but similar results have been observed in humans, as tenofovir usually does not affect the GFR, at least early in short-term exposition. In a study where the association

between tenofovir and GFR loss through years of cumulative exposure was evaluated, it was shown that the GFR loss is relatively mild in a long-term perspective (Laprise *et al*., 2012). Tenofovir is known to induce tubular dysfunction, and that seems to precede the decline in GFR (Fernandez-Fernandez *et al*., 2011) as several patients were reported to have tubular proteinuria even with normal GFR (Gatanaga *et al*., 2006).

As what it was reported by Peng *et al*. (2010), paracetamol induces severe morphological alterations in the glomerulus of zebrafish larvae. This may explain why in this assay, paracetamol-exposed larvae experienced such a high decrease in the glomerular function. Gentamicin, on the other hand, seems to induce reduced glomerular function by causing physical obstructions in the tubules. The presence of cellular residues in the tubules may increase the hydrostatic pressure inside the tubule and in the Bowmans' capsule, reducing the filtration gradient and, therefore, the GFR (Lopez-Novoa *et al*., 2011).

The lethality of injected larvae, summarized in the table 4, was lower among control larvae than drug-exposed larvae. That was to be expected, since drug-exposed larvae are weaker, because of the drug toxicity, than control ones. It was possible to notice, upon injection, that the tissues of drug-exposed larvae were weaker and softer, and that sometimes the injection damaged the blood vessels. This was especially visible in paracetamol and gentamicin exposed larvae (observed data, not shown), and it correlates with the higher lethalities percentage registered (table 4). Paracetamol and gentamicin also registered the highest lethalities upon exposure to the LC_{10} (table 3) of given drug, which could imply an initial weakness that got aggravated by the FITC-inulin injection. But given the fact that TDF registered a lethality upon LC_{10} exposure of 6.2%, a not so different value than the 11.2% of paracetamol, but only 2.8% lethality after injection, while paracetamol registered 44.3%, it is improbable that the different lethalties upon LC_{10} exposure and possible initial weakness contributed to the lethalies registered after injection.

Another interesting observation worth mentioning is that there was a higher variability in the FITC-intensity decay between drug-exposed larvae than control larvae, as the standard deviation was higher for the drug-exposed larvae (7.90 in controls versus 9.50 – 16.7 range in drug-exposed). This could be due to the fact that not only the n for control larvae was much higher (n=100) than for drug-exposure larvae (n=15-29), but also because some larvae might have absorbed higher amounts of drug than others, since the method of delivering the drug by soaking does not allow equally exact concentrations in each and every larvae (Kumar *et al*., 2013; Chaudhari *et al*., 2013), and/or just by the natural biological variability within larvae. Drugs could have been delivered by injection, as it was done in Hentschel *et al.* (2004) and Rider *et al.* (2012), but the possibility of decreasing the variability within larvae did not justify the increased workload, as the same treatment would have to be done throughout the rest of the experiments, nor did the increased larvae mortality by the injection procedure *per se*.

A weakness in this study is that larvae blood flow was not measured. This could be important because a higher blood flow would mean a higher amount of blood passing through the glomeruli, which could result in a higher FITC-inulin clearance rate, and *vice-versa* for a decreased blood flow. Similarly, cilia beat frequencies were not measured either. Cilia are present along and inside the ducts of the kidney mediating the fluid flow (Zhao and Malicki, 2007). It would be interesting to measure these two parameters, as it would give more information on whether the differences in the clearance rate of inulin are due to glomeruli degradation alone, for example, or also because of differences in the blood flow and/or cilia beat frequency.

3. Transmission Electron Microscopy

If one wants to see what is actually happening inside a cell, TEM is certainly one of the best approaches. Depending on the sample treatment, it allows us to see several cell structures and organelles, from large structures such as the nucleus and mitochondria, till much smaller ones, such as nucleosomes and ribosomes (Fawcet, 1981). Proximal tubule cells, even though they contain large numbers of mitochondria, are intrinsically vulnerable to mitochondrial dysfunction because of limited anaerobic ATP-generating capacity and a relative high demand in ATP for the active reabsorption of filtered nutrients and ions (Abraham *et al*., 2013; Ramamoorthy *et al*., 2014;). That may explain why nephrotoxicity induced by tenofovir mainly occurs in the convoluted tubules zones, since the primary targets seem to be the mitochondria. On that matter, sections from the convoluted tubules zone from zebrafish larvae were cut to be analyzed by TEM.

It should be noted, though, that 2D micrographs could be a little dubious regarding mitochondria and cristae "true" shape, volume and number. The classic "textbook" view of mitochondria as bean-shaped organelles with a highly dense and packed cristae has been challenged by the introduction of 3D reconstructing technologies (Karbowiski and Youle, 2003; Rafelski, 2013). Extensive and physically interconnected networks formed by the mitochondria have been observed and reported to date (De Giorgi *et al*, 2000; Skulachev, 2001), and they may serve the purpose of an efficient system to deliver energy, or channel calcium between different areas of the cell (Karbowiski and Youle, 2003). As it is, mitochondria and cristae shape can critically vary depending on the position on the cut of the section and the position of the mitochondria itself on the cell. Still, every cell from every part of the tubule was observed (over 50 cells per condition) so it was possible to have a very good estimative regarding mitochondria and cristae overall shape by looking at the 2D micrographs.

To overcome the limitations of 2D micrographs to evaluate the mitochondrial volume, we considered performing a stereology analysis[12], a relatively simple and low time consuming method (Reid, 1981; Weibel, 1979). However, this is a fairly archaic and a no longer used method, as well as that it could only give an approximated volume and it could not add any information regarding mitochondria and cristae overall shape. As it was, this approach was discarded.

Then, a 3D cell model and a 3D mitochondria model from TFV-exposed and control larvae were constructed, and volumes from the several structures within each model were obtained and compared against each other. Due to the complexity of this technique, only one cell and mitochondrion was modeled. Hence, because of the reduced sample size, a statistical analysis could not be performed, and therefore no final conclusions can be taken. However, interesting differences were observed between the 2 modelled cells and mitochondria.

The 2D micrographs (Fig. 16) showed that gentamicin-exposed larvae had the most altered phenotype regarding mitochondria appearance, while the paracetamol-exposed larvae the less altered, with TDF and TFV, with similar patterns, in the middle. Whether TFV or TDF -exposed larvae (Fig. 16.4 and 16.5) showed any differences between them was inconclusive; albeit TFV appeared to have a higher amount of altered mitochondria, this observation might be purely subjective and/or insignificant. It should be noted, though, that although the drug concentrations used were all the ones corresponding to the previously calculated LC_{10}, gentamicin-exposed larvae registered a 16.67% mortality, while paracetamol, TDF or TFV -exposed larvae had only 0% mortality (Table 5). This difference could explain the high alteration pattern encountered in the gentamicin-exposed larvae, but since only one exposition replicate was performed on the larvae, this observation is merely speculative.

In gentamicin, TDF or TFV -exposed larvae mitochondria appeared swollen when compared to the ones from the control larvae (Fig. 16.2, 16.4 and 16.5, respectively), as they were much larger and lighter. Mitochondrial swelling is considered to be a sign of a deteriorated function of the organelle (Abraham *et al*., 2013), which could be due to increased permeability of the inner mitochondrial membrane to solutes (Ramamoorthy *et al*., 2014). Also, cristae appeared disrupted in the 2D micrographs (Fig. 16.2, 16.4 and 16.5) and in the tomogram from the TFV-exposed larvae mitochondrion it was possible to distinguish small spheres that appeared to be cristae remains, as well as a clear reduction in cristae branching and network (Fig. 23. 2). Mitochondria are the energy source of the cell, as the cristae contains the components of the electron transport chain (ETC), the main responsible for ATP synthesis. Damage to the cristae can result in a disruption of the ECT, leading to a decreased activity of the electron chain complexes that culminates in a decrease in the ATP production (Ramamoorthy *et al*., 2014). Also, a

[12] This method relays on the placement of equally spaced points over a micrograph and the identification of the structure where each point lays. A score is then attributed to each micrograph and relative percentages of each structure can be calculated per micrograph, including mitochondria and cristae volumes (Reid, 1981; Weibel, 1979).

smaller extension of the cristae also implies a reduced ATP synthesis capacity. This results suggest that the mitochondria and their capacity to generate ATP in gentamicin, TDF or TFV -exposed is clearly impaired.

Other animal models have also been exposed to tenofovir and similar observations have been reported (Abraham *et al*., 2013; Kohler *et al*., 2009; Ramamoorthy *et al*., 2014). Abraham *et al*. (2013) and Ramamoorthy *et al.* (2014) reported extensive proximal tubular mitochondrial injury, revealed by electron microscopy, in rats that had been chronically exposed to TDF. But in addition to swollen mitochondria with irregular shapes and disrupted cristae, they also observed an accumulation of amorphous deposits in the mitochondrial matrix. Electron microscopy reports performed on HIV patients on antiretroviral therapy with tenofovir have also showed widespread morphological abnormalities in proximal tubule mitochondria, with variations in size, shape, disruption of cristae, mitochondrial swelling and the presence of intramitochondrial paracrystals (Herlitz *et al*., 2010). Mitochondrial deposits were not observed in our zebrafish larvae mitochondria, unless the so called cristae remains observed in the tomogram were indeed the amorphous deposits and/or intramitochondrial paracrystals, whose nature still remains to be found. Also, although it should not be an issue, the tomogram was of a mitochondrion from a larvae that had been acutely exposed to TFV, while the reports were all of a chronic exposition to TDF.

Houghton *et al.* (1976) and Cui *et al*. (2015) reported similar findings, regarding mitochondria phenotype, in gentamicin-exposed rats and mini-pigs, respectively. Large, swollen mitochondria with disrupted cristae were seen in the convoluted tubules cells, although no reference was made regarding the presence, or absence, of matrix granules.

Gentamicin is reabsorbed mainly in the proximal convoluted tubule and accumulates mostly in the lysosomes, Golgi apparatus and endoplasmic reticulum. Gentamicin binds to membrane phospholipids, alters their turnover and metabolism and, as consequence, causes phospholipidosis (Lopez-Novoa, 2011), what we referred as membrane deposits. This condition has been observed in humans (Broe *et al.*, 1984) and experimental animals (Giuliano *et al*., 1984; Nonclercq *et al*., 1992). And, indeed, a higher presence of membranes deposits was registered in the gentamicin-exposed larvae when compared to the controls and other drugs (Fig. 16.2, 1k magnification).

Paracetamol-exposed larvae exhibited either small clusters of small mitochondria or long and thin mitochondria rather than the swollen phenotype observed in the gentamicin, TDF or TFV -exposed larvae (Fig. 16.3). Ruepp *et al.* (2001) also reported, in mice exposed to paracetamol, large mitochondria that appeared to be fused together rather than swollen. The formation of short, round mitochondria has been associated with mtDNA depletion or treatment with mitochondrial toxins, and is most likely regulated by the rates of fusion and fission events. Fusion and fission events, commonly referred as mitochondrial dynamic events, occur constantly and naturally within a cell. But cell stresses can push

this dynamic either to an increase of fission events over fusion, or the opposite. If fusion is increased over fission, mitochondria join forming a single mitochondrial network. Fusion allows the mixing of oxidatively damaged mitochondrial contents, generated as a byproduct of respiration, allowing the restoration of the damaged mitochondria when it re-fuses to the network. Fission, on the other hand, creates continuous small fragments that can undergo mitophagy if excessively damaged (Rafelski, 2013). On this regard, paracetamol seems to induce more fission events than fusion, as the amount of short mitochondria was more commonly seen than long ones. The 3D cell model, when finished, should clarify this issue.

The 2D micrographs, as well as the 3D cell model, showed the presence of several damaged mitochondria, which appeared as "white spots". Several mitochondria were being phagocyted by lysosomes and/or peroxisomes (Fig. 18.4 and 20). These mitochondria were most likely undergoing mitophagy (mitochondrial autophagy), a normal process in cells. The mitochondria population within a cell is naturally controlled by biogenesis (creation of new mitochondrial material) and mitophagy. But mitophagy can also be induced by a variety of stresses, thus decreasing the mitochondria population (Rafelski, 2013). Since the presence of damaged mitochondria was more commonly seen in drug-exposed larvae than in controls, it can be assumed that the toxicity caused by these drugs induced mitophagy, so it is possible that the mitochondria population is reduced. The mitochondria volume occupied in 3D cell model of the TFV-exposed larvae cell was indeed lower than the control one (Fig. l.4), but since a statistical analysis could not be performed, no conclusions can be taken.

Mitochondrial matrix granules are osmiophilic[13] and usually measure 20–50 nm in diameter (Manov *et al.*, 2006). Its importance in the mitochondria metabolism is still poorly understood, but they are believed to be calcium phosphate deposits (Boonrungsiman *et al*., 2012) and to have a role in the calcium metabolism (Manov *et al.*, 2006). Variations in matrix granules frequency have been previously associated with drug toxicity (Manov *et al*., 2004). Here it was registered a partial loss of matrix granules in paracetamol-exposed larvae and a complete loss in gentamicin, TDF or TFV -exposed larvae. It seems to be that loss in matrix granules is a sign of drug toxicity and it could be associated with an increased requirement of calcium by the mitochondria.

Mitochondria polarity was not affected by the different conditions and when compared to the controls. Mitochondria usually appeared in the lateral and basal side of the cells and, occasionally, 1-2 mitochondria appeared in the apical side as well. This pattern was constant for all conditions.

An interesting observation was that the RER was much more regularly seen, and longer when present, in drug-exposed larvae, regardless of the drug nature (differences were not sufficiently apparent) than in controls. Gentamicin (Houghton *et al*., 1976), aspirin, and paracetamol (Manov *et al*., 2004) have

[13] They are only stained by the osmium solution (Manov *et al*., 2004).

been previously shown to dilate the RER as well. The RER is the major site of protein synthesis (Manov *et al*., 2004) and it is usually more abundant in cells that synthetize large amounts of proteins for export as a secretory product (Fawcet, 1981). This results suggest that cells could be either responding to the drug-toxicity imposed stress by increasing protein production or that the RER is dilated in semblance with the mitochondria, by an increase in the membrane permeability to solutes.

Regarding the cell's nucleus, no apparent differences were found in heterochromatin and euchromatin presence or disposition along the nucleus from the larvae cells. Nucleus from drug-exposed larvae appeared a little swollen when compared to controls. Although no conclusions can be made regarding differences registered by the 3D cells models, because of insufficient n, the TFV-exposed larvae cell nucleus had indeed a higher volume, 26.20%, than the control. Different observations have been noted regarding nucleus size in drug-exposed animals; in Abraham *et al.* (2013) nucleus in TDF-exposed rats appeared shrunken, in Houghton *et al.* (1976) gentamicin-exposed rats' nucleus appeared enlarged and in Kohler *et al.* (2009) TDF-exposed mice nucleus seemed intact.

It was not possible to distinguish whether the lumen was swollen or not, and if it varied with the different conditions, since the tubules outer shape varied considerably depending on their position in relation to where the cut of the section was performed (data not shown). But several studies, as well as some experiments that are undergoing in the laboratory, have shown that the lumen increases in size when exposed to toxic drugs.

No differences in the cilia structure were found between the different conditions. It should be noted, though, that cilia often showed blurred in the micrographs, so it was possible that some cilia might had had some milder alterations that were not distinguished because of said blurriness. To overcome this issue, micrographs would have had to be taken under different capture angles, since cilia were not always captured perpendicular to the section cut. But since this would significantly increase the workload and cilia were not the main focus on this thesis, this was not performed.

A surprising new information that the tomograms added was the presence of what appeared to be cristae remains from the cristae fragmentation on the mitochondrion from the TFV-exposed larvae. These structures were not identified in the micrographs, probably because without the possibility of investigating the previous and/or the next micrographs they were disguised as small cristae bumps. Another unexpected addition was the appearance of matrix granules in the same tomogram, as no mitochondrion from the thoroughly investigated TFV-exposed larvae cells in the 2D micrographs showed any. That could be just happenstance that no matrix granule showed in the micrographs, as they only accounted 0.01% of the mitochondrion volume. But there is also, and perhaps more probable, possibility that some of the identified matrix granules in the tomogram were wrongly identified as they could have, in fact, been smaller and compacted cristae remains. If so, the matrix granules percentage could be overestimated in this tomogram.

Because the electron microscope did not take a micrograph from every single angle – from -90º till +90º (microscope limitations) – some portions of the mitochondria membranes, including cristae, inner and outer membrane, were not captured by the micrographs and, therefore, could not be visualized and included in the model. For that reason, models might be underestimated regarding cristae. But this phenomenon is consistent for all conditions, therefore models from controls and drug-exposed larvae can still be compared to each other with a high measure of accuracy. On that matter, it was not always possible to distinguish the inner form the outer membrane either, hence the reason why the model did not had both membranes distinguished. But since it was clear that they were always relatively close and did not distanced much from each other, a single contour representing both membranes could be drawn with high precision. Besides, no apparent differences were found between control and TFV-exposed larvae, regarding the distance between both membranes, which means that fluids, in TFV-exposed larvae where swelling took place, did not get retained in the intermembrane space.

Every membrane captured by the micrographs showed a little "wavy". This is possibly an artifact caused by the samples treatment with the microwave procedure. Membranes should appear normal if a more conventional procedure were to be used, such as by RT (room temperature) sample preparation.

It can be argued that the n used for TEM was too low, since only one drug-exposition replicate was performed and only one larvae per TEM analysis (2D micrographs, serial sequences and tomography) was observed. But that means that a total of three larvae per condition was observed, and regardless of the TEM analysis later performed, all sections were strictly screened and the same observations were noted on all larvae per condition. To include more replicates and more larvae per TEM analysis would mean an increased workload, which could not be accomplished in this thesis duration period.

Conclusions and future perspectives

Several main conclusions can be taken upon the results of this thesis:

1. Of the four studied nephrotoxic drugs, gentamicin is the most powerful in terms of lethality, followed by TDF, TFV and lastly paracetamol, the less toxic;
2. Taking into account the slopes of the lethality curves, gentamicin has a very different mechanism of drug toxicity compared to TDF, TFV or paracetamol;
3. Paracetamol was the drug that induced the highest decrease in glomerular function, followed by gentamicin; while both proved to be reliant positive controls to assess renal function, gentamicin could be a more sensitive control;
4. Neither TDF nor TFV altered the glomerular function at LC_{10} concentrations;
5. Gentamicin, TDF and TFV caused severe ultrastructural mitochondrial alterations, showing swelling, irregular shapes, cristae disruption and a complete loss of matrix granules;
6. Paracetamol caused milder ultrastructural mitochondrial alterations, showing mitochondria undergoing fission and fusion, mild cristae disruption and partial loss of matrix granules;
7. A 3D cell model of a TFV-exposed larvae showed a decreased mitochondria network, with less branching mitochondria and less mitochondria volume, which could suggest an increase in mitophagy;
8. A 3D mitochondrion model of a TFV-exposed larvae showed a decreased cristae network and presence of cristae remains, which suggests an impaired electron transport chain and, therefore, an impaired capacity of ATP synthesis.

Future work should be done, though, in order to better proof the reliability of this model and to better characterize it:

A. TEM: more 3D models will have to be done, both of serial sequences and tomograms, so that a statistically analysis can be performed. Also, a second exposition on larvae to be analyzed by TEM should also be performed, to look for and confirm replicable results;
B. Mitochondrial DNA: mitochondrial DNA of drug-exposed larvae needs to be quantified to have a quantitative measure of mitochondrial population and to evaluate the impact of tenofovir on DNA polymerase gamma;
C. Glomerular function: drug-exposed larvae heart beat should be measured, as well as the cilia beat frequency, to better understand the FITC-inulin clearance assay results;
D. Immunohistochemistry: PCNA (Proliferating Cell Nuclear Antigen) immunohistochemistry and a TUNEL (Terminal deoxynucleotidyl transferase dUTP nick end labeling) assay should

also be performed on the convoluted tubules sections, to evaluate cell proliferation and cell death, respectively;

E. Dose-dependent results: a 2nd experiment series should be performed with a lower drug concentration, to explore for possible dose-dependent results;
F. Chronic drug exposition: it would be interesting to perform the same analysis on larvae with a chronic drug-exposition regime, since HIV patients follow chronic drugs-based treatments.

All in all, this study allowed us to understand that zebrafish larvae can be, indeed, a good animal model to assess the functional and structural damage associated with DIRI. The function and morphological alterations obtained after treatment with the different nephrotoxic drugs were similar to those found in humans, so that results so far are promising. Therefore, zebrafish larvae could be a good first choice when first approaching animal models, as they could be used to screen a fair amount of new drugs and characterize its effects before resorting to more expensive and complex animal models.

References

Abraham, P., Ramamoorthy, H., Isaac, B. 2013. Depletion of the cellular antioxidant system contributes to tenofovir disoproxil fumarate - induced mitochondrial damage and increased oxido-nitrosative stress in the kidney. Journal of Biomedical Science. 20:61

Arambaši, M. B. and Randhawa, M. A. 2014. Comparision of the Methods of Finney and Miller-Tainter for the Calculation of LD50 Values. World Applied Sciences Journal 32 (10): 2167-2170.

Arambasié, M., Randhawa, M. 2014. Comparison of the Methods of Finney and Miller-Tainter for the Calculation of LD Values. World Applied Sciences Journal. 32 (10): 2167-2170.

Arts, E. J., Hazuda, D. J. 2012. HIV-1 Antiretroviral Drug Therapy. Cold Spring Harb Perspect Med. 2:a007161.

Bae, J. W., Guyer, W., Grimm, K., Altice, F. 2011. Medication persistence in the treatment of HIV infection: a review of the literature and implications for future clinical care and research. AIDS. 25: 279-290.

Balakumara, P., Rohillab, A., Thangathirupathia, A. 2010. Gentamicin-induced nephrotoxicity: Do we have a promising therapeutic approach to blunt it?

Banote, R. K., Koutarapu, S., Chennubhotla, K. S., Chatti, K. and Kulkarni, P. 2013. Epilepsy & Behavior 27: 212-219.

Barré-Sinoussi, F., Ross, A., Delfraissy, J. 2013. Past, present and future: 30 years of HIV research. Perspectives, Nature Reviews. MicrobioIogy. 11: 877-883.

Berns, J., Kasbekar, N. 2006. Highly Active Antiretroviral Therapy and the Kidney: An Update on Antiretroviral Medications for Nephrologists. Clinical Journal of the American Society of Nephrology. Clin J Am Soc Nephrol. 1: 117–129.

Blüthgen, N. 2014. Effect of UV filter (benzophenones an octocrylene) and mifepristone on different life stages of zebrafish (*Danio rerio*). 298 pp.

Boonrungsimana, S., Gentlemana, E., Carzanigad, R., Evansa, N., McComba, D., Portera, A., Stevensa, M. 2012. The role of intracellular calcium phosphate in osteoblast-mediated bone apatite formation. PNAS. 109 (35): 14170-14175.

Brady, M. T., Oleske, J. M., Williams, P. L., et al. 2010. Declines in mortality rates and changes in causes of death in HIV-1- infected children during the HAART era. Journal of Acquired Immune Deficiency Syndromes. 53 (1): 86–94.

Broe, M., Paulus, G., Verpooten, G., Roeles, F., Buyssens, N., Weddedn, R., Van Hoof, F., Tulkens. 1984. Early effects of gentamicin, tobramycin, and amikacin on the human kidney. Kidney International 25: 643—652.

Catalfamo, M., Wilhelm, C., Tcheung, L., Proschan, M., Friesen, T., Park, J., Adelsberger, J., Baseler, M., Maldarelli, F., Davey, R., Roby, G., Rehm, C., Lane, C. 2014. CD4 and CD8 T Cell Immune Activationuring Chronic HIV Infection: Roles of Homeostasis, HIV, Type I IFN, and IL-7.

Chaudhari, G. H., Chennubhotla, K. S., Chatti, K. and Kulkarni, P. 2013. Journal of Pharmacological and Toxicological Methods. 67: 115-120.

Cheng, C., Verdun, V., Wingert, R. 2015. Recent Advances in Elucidating the Genetic Mechanisms of Nephrogenesis Using Zebrafish. Cells. 4: 218-233

Cudd, T. 2005. Animal Model Systems for the Study of Alcohol Teratology. Exp Biol Med (Maywood). 230 (6): 389-393.

Cui, J., Bai, X., Sun, X., Cai, G., Hong, Q., Ding, R., Chen, X. 2015. Rapamycin protects against gentamicin-induced acute kidney injury via autophagy in mini-pig models. Sci. Rep. 5: 11256.

Dooley, K. and Zon, L. I. 2000. Zebrafish: a model system for the study of human disease. Current Opinion in Genetics and Development. 10: 252–256.

Drummond and Joseph V. Bonventre, D., Bonventre J., Hentschel, D., Moo Park, K., Cilenti, L., Zervos, A. 2004. Acute renal failure in zebrafish: a novel system to study a complex disease. Am J Physiol Renal Physiol. 288: F923-F929.

Drummond, I and Davidson, A. 2010. Zebrafish kidney development. Methods in Cell Biology. 100: 233-260.

Drummond, I., majumdar, A., Hentschel, H., *et al*. 1998. Early development of the zebrafish pronephros and analysis of mutations affecting pronephric function. Development. 125: 4655-4667.

Fawcet, D. W. 1981. The Cell. 2nd edition. W. B. Saunders Company. Munich, Germany

Fernandez-Fernandez, B., Montoya-Ferrer, A., Sans, A. B., et al. 2011. Tenofovir Nephrotoxicity: 2011 Update. AIDS Research and Treatment. 2011. 11p.

Fischer, M. J., Wyatt, C. M., Gordon, K. et al.. 2010. Hepatitis C and the risk of kidney disease and mortality in veterans with HIV. Journal of Acquired Immune Deficiency Syndromes. 53 (2): 222–226.

Gallant, J. E., Staszewski, S., Pozniak, A. L., et al. 2004. Efficacy and safety of tenofovir DF vs stavudine in combination therapy in antiretroviral-naive patients: a 3-year randomized trial. Journal of the American Medical Association. 292 (2): 191–201.

Gatanaga, H., Tachikawa, N., Kikuchi, Y., et al.. 2006. Urinary _2-Microglobulin as a Possible Sensitive Marker for Renal Injury Caused by Tenofovir Disoproxil Fumarate. AIDS RESEARCH AND HUMAN RETROVIRUSES. 22 (8): 744-748.

Geboers, S., Haenen, S., Mols, R., *et al*. Intestinal behavior of the ester prodrug tenofovir DF in humans. 21 pp.

Gelder, J. Van, Deferme, S., Naesens, L., Clercq, E. de, Mooter, G. Van Den, Kinget, R. and Augustijns. 2002. Intestinal Absorption Enhancement of the Ester Prodrug Tenofovir disoproxil Fumarate through Modulation of the Biochemical Barrier by Defined Ester Mixtures. Drug Metabolism and Disposition. 30: 924-930.

Gerard, L. Chazallon, C., Taburet, A-M., et al. 2007. Renal function in antiretroviral-experienced patients treated with tenofovir disoproxil fumarate associated with atazanavir/ritonavir. Antiviral Therapy. 12: 31-39.

Gerhard, G. S., Kauffman, E. J., Wang, X., Stweart, R., Moore, J. L., Kasales, C. J., Demidenko, E., Chengo, K. C. 2002. Life spans and senescent phenotypes of zebrafish (*Danio rerio*). Experimental Gerontology. 37: 1055-1068.

Gerlach, G and Wingert, R. 2013. Kidney organogenesis in the zebrafish: insights into vertebrate nephrogenesis and regeneration. Wiley Interdiscip Rev Dev Biol. 2(5): 559–585.

Gerntholtz, T. E., Goetsch, S. J. W., Katz, I. HIVrelated nephropathy: a South African perspective. 2006. Kidney International. 69 (10): 1885–1891.

Giorgi, F. Ichas, L. 2000. Electrical coupling and plasticity of the mitochondrial network. Cell Calcium. 28 (5/6) 365–370.

Giuliano, R., Paulus, G., Verpooten, G., Pattyn, V., Pollet, D., NOUWEN, E., Laurent, G.,Carlier, M., Maldague, P., Tulkens, P., De Broe, M. 1984. Recovery of cortical phospholipidosis and necrosis after acute gentamicin loading in rats. Kidney International. 26: 838—847.

Goedea, A.,Vultob, A., Osterhausa,A., Gruters, R. 2014. Understanding HIV infection for the designof a therapeutic vaccine. Part I: Epidemiology and pathogenesis of HIVinfection.

Hentschel, D., Mengel, M., Boehme, L., Liebsch, F., Albertin ,C., Bonventre, J., Haller, H., Schiff, M. 2007. Rapid screening of glomerular slit diaphragm integrity in larval zebrafish. Am J Physiol Renal Physiol. 293: F1746-F1750.

Hentschel, D., Park, K., Cilenti, L. et al. 2005. Acute renal failure in zebrafish: a novel system to study a complex disease. Am J Physiol Renal Physiol 288: F923–F929.

Herlitz, L., Mohan S., Stokes, M., Radhakrishnan, J., D'Agati, V., Markowitz, G. 2010. Tenofovir nephrotoxicity: acute tubular necrosis with distinctive clinical, pathological, and mitochondrial abnormalities. Kidney International. 78: 1171–1177.

Horsfiel, J., Ramachandran, A., Reuter, K., et al. 2002. Cadherin-17 is required to maintain pronephric duct integrity during zebrafish development. Mechanisms of Development. 115: 15–26

Houghton, D., Hartnett, M., Campbell-Boswell, M., Porter, G., Bennett, W. 1976. A Light and Electron Microscopic Analysis of Gentamicin Nephrotoxicity in Rats. American Journal of Pathology. 82:589-612.

Islam, M., Wu, J., Jansson, J., Wilson, D. 2012. Relative risk of renal disease among people living with HIV: a systematic review and meta-analysis. http://www.biomedcentral.com/1471-2458/12/234

Jayaram, K. C. 1999. The freshwater fishes of the Indian region. Narendra Publishing House, Delhi.

Kaiser Family Foundation. 2015. Filling the need for trusted information on national health issues. 1-4.

Kalyesubula, R., Perazella,M. 2011. Nephrotoxicity of HAART. Hindawi Publishing Corporation AIDS Research and Treatment. 2011: 11pp.

Karbowski, M., Youle, R. 2003. Dynamics of mitochondrial morphology in healthy cells and during apoptosis. Cell Death and Differentiation .10, 870–880.

King, T., Bushman, L., Kiser, J., Anderson, P. L., et al. 2006. Liquid chromatography–tandem mass spectrometric determination of tenofovir-diphosphate in human peripheral blood mononuclear cells. Journal of Chromatography B. 843: 147–156

Kohler, J., Hosseini, S., Hoying-Brandt, A., Green, E.,Johnson, D., Russ, R., Tran, D., Raper, M., Santoianni, R., Lewis, W. 2009. Tenofovir renal toxicity targets mitochondria of renal proximal Tubules. Lab Invest. 89(5): 513–519.

Laprise, C., Baril, J.-G., Dufresne, S., Trottier, H. 2012. Association Between Tenofovir Exposure and Reduced Kidney Function in a Cohort of HIV-Positive Patients: Results From10 Years of Follow-up. Clinical Infectious Diseases Advance Access. 1-9

Laurence, C. 2007. The husbandry of zebrafish (Danio rerio): A review. Aquaculture 269: 1–20.

Levey, A. S., Coresh, J., Bolton, K., et al. 2002. K/DOQI clinical practice guidelines for chronic kidney disease: evaluation classification, and stratification. American Journal of Kidney Diseases, 39,1 (2): S1–S266.

Lister, J., Robertson, C., Lepage, T., et al. 1999. nacre encodes a zebrafish microphthalmia-related protein that regulates neural-crest-derived pigment cell fate. Development 126, 3757-3767.

Lopez-Novoa, J., Quiros, Y., Vicente L., Morales, A., Lopez-Hernandez, F. 2011. New insights into the mechanism of aminoglycoside nephrotoxicity: an integrative point of view. Kidney International. 79: 33–45.

Mann, J. 1987. AIDS – A global perspective. West J Med. 147: 732-734.

Manov, I., Hirsh, M., Iancu, T. 2004. N-Acetylcysteine does not Protect HepG2 Cells against Acetaminophen-Induced Apoptosis. Basic & Clinical Pharmacology & Toxicology. 94: 213–225.

Matthews, M., Trevarrow, B., Matthews, J. 2002. A virtual tour of the guide for zebrafish users. Lab. Anim. 31: 34-40.

Moss, D., Neary, M., Owen, A. 2007. The role of drug transporters in the kidney: lessons from tenofovir. Front. Pharmacol. 5:248.

Müller, M., Wandel, S., Colebunders, R., Attia, S., Furrer, H., Egger, M. 2010. Immune reconstitution inflammatory syndrome in patients starting antiretroviral therapy for HIV infection: a systematic review and meta-analysis. Lancet Infect Dis. 10: 251–61.

Nelson, M. R., Katlama, C., Montaner, J. S., et al. 2007. The safety of tenofovir disoproxil fumarate for the treatment of HIV infection in adults: the first 4 years. AIDS 21. (10): 1273–1281.

Nonclercq, D., Wrona, S., Toubeau, G., Zanen, J., Heuson-Stiennon, J., Schaudies, P., Laurent, G. 1992.Tubular Injury and Regeneration in the Rat Kidney Following Acute Exposure to Gentamicin: A Time-Course Study. Renal Failure. 14(4): 507-521.

Ortiz, A., Justo, P., Sanz, A., et al. 2005. Tubular cell apoptosis and cidofovir-induced acute renal failure. Antiviral Therapy. 10 (1): 185–190.

Panel on Antiretroviral Guidelines for Adults and Adolescents. Guidelines for the use of antiretroviral agents in HIV-1-infected adults and adolescents. Department of Health and Human Services. Available at http://www.aidsinfo.nih.gov/ContentFiles/AdultandAdolescentGL.pdf. Accessed 20.09.15

Peçanha, E. P., Antunes, O. 2002. ESTRATÉGIAS FARMACOLÓGICAS PARA A TERAPIA ANTI-AIDS. Quim. Nova. 25 (6B): 1108-1116.

Peng, H., Wang, Y., Wen, C., Wang, W., Cheng, C., Chen, Y. 2010. Nephrotoxicity assessments of acetaminophen during zebrafish embryogenesis.

Perner, B., Englert, C., Bollig, F. 2007. The Wilms tumor genes wt1a and wt1b control different steps during formation of the zebrafish pronephros. Developmental Biology 309: 87–96.

Pollok, R. C. G., Francis, N., Cliff, S., Nelson, N., Gazzard, B. 1995. Kaposi's sarcoma in the kidney. International Journal of STD and AIDS. 6 (4): 289–290.

Quinn KJ. 2010. Incidence of proximal renal tubular dysfunction inpatients on tenofovir disoproxil fumarate. Int J STD AIDS. 21:150–151.

Rafelski, S. 2013. Mitochondrial network morphology: building an integrative, geometrical view. BMC Biology. 11:71

Ramamoorthy, H., Abraham, P., Isaac, B. 2014. Mitochondrial Dysfunction and Electron Transport Chain Complex Defect in a Rat Model of Tenofovir Disoproxil Fumarate Nephrotoxicity. J Biochem Molecular Toxicology. 28 (6).

Randahawa, M. A. 2009. Calculation of LD50 values from the method of Miller and Tainter, 1944. J Ayub Med Coll Abbottabad 21(3): 184-185.

Reid, A., St¨ohr, W., Walker, A. S. et al. 2008. Severe renal dysfunction and risk factors associated with renal impairment in HIV-infected adults in Africa initiating antiretroviral therapy. Clinical Infectious Diseases. 46 (8) 1271–1281.

Rider, S., Tucker, C., del-Pozo, J., Rose, K., MacRae, C., Bailey, M., Mullins, J. 2012. Techniques for the in vivo assessment of cardio-renal function in zebrafish (Danio rerio) larvae. The Journal of Physiology. J Physiol. 590.8: 1803–1809.

Rodriguez-Novoa S. Critical appraisal and update on tenofovir in management of human immunodeficiency virus infection. 2011. Virus Adapt Treat. 55.

Roe, J., Campbell, L. J., Ibrahim, F., Hendry, B. M., Post, F. A. 2008. HIV care and the incidence of acute renal failure. Clinical Infectious Diseases. 47 (2): 242–249.

Ruepp, S., Tonge, R., Shaw, J., Wallis, N., Pognan, F. 2001. Genomics and Proteomics Analysis of AcetaminophenToxicity in Mouse Liver. TOXICOLOGICAL SCIENCES. 65: 135–150

Schmatz, D., Romancheck, M., Pittarelli L., Schwartz, R., Fromtling, R., Nollstadt, K., Vanmiddlesworth, F., Wilson, K., Turner, M. 1990. Treatment of Pneumocystis carinji pneumonia with 1,3-f3-glucan synthesis inhibitors. Medical Sciences. 87: 5950-5954.

Skulachev, V. Mitochondrial filaments and clusters as intracellular power-transmitting cables. Trends in Biochemical Sciences. 26 (1): 23–29.

Spence, R., Gerlach, G. Lawrence, C., Smith, C. 2008.The behaviour and ecology of the zebrafish,Danio rerio. Biol. Rev. 83: 13–34.

Stark, J. D. and Banks, J. E. 2003. Population-Level Effects of Pesticides and other Toxicants on Arthropods. Annu. Rev. Entomol. 48: 505–519.

Sterba, G. 1962. Freshwater fishes of the world. Vista Books, Longacre Press, London.

Szczech, L. A., Gupta, S. K., Habash, R. et al. 2004. The clinical epidemiology and course of the spectrum of renal diseases associated with HIV infection. Kidney International. 66 (3): 1145–1152.

Talwar, P. K. and Jhingran, A. G. 1991. Inland fishes of India and adjacent countries. Oxford & I. B. H. Publishing, Calcutta.

Tamkus, D., Jajeh, A., Osafo, D., Hadad, L., Bhanot, B., Yogore, M. G. 2006. Thromboticmicroangiopathy syndrome as an AIDS-defining illness: the experience of J. Stroger Hospital of Cook County. Clinical Advances in Hematology and Oncology. 4 (2): 145–149.

The Henry J. Kaiser Family Foundation. 2015. Fact sheet. The Global HIV/AIDS Epidemic.

The rgp120 HIV Vaccine Study Group. 2004. Placebo-Controlled Phase 3 Trial of a Recombinant Glycoprotein 120 Vaccine to Prevent HIV-1 Infection. The Journal of Infectious Diseases. 191:654–6

Tsai, W., Wang, L., Hsu, Y., Lin, y., Fang, T., Hsu, B. 2014. enofovir nephropathy in a patient with human immunodeficiency virus. Tzu Chi Medical Journal.

UNAIDS. 2014. 2014 report on AIDS.

UNAIDS. 2015. How AIDS changed everything. Executive Summary.

UNGASS. 2001. Keeping the promise – Summary of the Declaration of Commitment on HIV/AIDS.

United Nations. 2011. General Assembly – public declaration.

Wakefield, A., Peters, S., Banerji, S.,Bridge, P., Hall, G., Hawksworth, D.,Guiver, L. Allen, A., Hopkin, J. 1992. Pneumocystis car/n/V shows DNA homology with theustomycetous red yeast fungi. MolecularMicrobiology. 6 (14): 1903-1911.

Walker, B, Burton, D. 2008. Toward an AIDS Vaccine. Science. 320 (5877):760-764.

Watanabe, N., Kato, M.,Suzuki, N., Inoue, C., Fedorova, S., Hashimoto, H., Maruyama, S., Matsuo, S., Wakamatsu, Y. 2009. Kidney regeneration through nephron neogenesis in medaka. Journal compilation.

Weibel, E. 1979. Stereological Principles for Morphometry in Electron Microscopic Cytology.

Weibel, E. Stereological principles for morphometry in electron microscopic cytology. 1979. Int Rev Cytol. 26:235–302.

White, R., Sessa, A., Burke, C., et al. 2008. Transparent Adult Zebrafish as a Tool for In Vivo Transplantation Analysis Cell Stem Cell. 2: 183–189.

WHO. 1997. WHO global programme on AIDS.

WHO. 2015. WHO statistics 2015.

Winiarczyk M, Sikora A, Mikuta T, Wiercińska-Drapato A. 2009. Nephrotoxicity of Tenofovir true or myth? HIV AIDS Rev. 8 (3):17–20.

Wyatt, C. M., Malvestutto, C., Coca, S. G., Klotman, P. E., Parikh, C. R. 2008. The impact of hepatitis C virus infection on HIV-related kidney disease: a systematic review and metaanalysis, AIDS. 22 (14): 1799–1807.

Zhao, C., Malicki. J. 2007. Genetic defects of pronephric cilia in zebrafish. Mechanisms of Development.124: 605–616.

Zhou, W., Boucher, R., Bollig, F., Engelrt, C., Hildebrandt, F. 2010. Characterization of mesonephric development and regeneration using transgenic zebrafish. Am J Physiol Renal Physiol. 299: F1040-F1047.

Internet:

http://www.avert.org/ (10.08.2015)

http://zebrafishart.blogspot.pt/ (Lizzy Griffins, 24.08.2015)

http://zfin.org/ (15.08.2015)

https://aidsinfo.nih.gov/ (10.08.2015)

https://www.aids.gov/ (10.08.2015)

Annexes

I. Recipes

Embryo Medium (EM) (500 mL): 10 mL E3 50x, 10 mL HEPES 500mM, NaOH til pH=7.40, H_2O MiliQ til 500 mL

EPON-resin (15 mL): 14.04 g EPON I, 18.09 g EPON II, 0.49 mL DMSO

Fixation solution: 2.5% glutaraldehyde, 2% PFA in 0.1M PHEM Buffer

HEPES (500 mM) (100 mL): 11.915g HEPES, 100 mL H_2O MiliQ

Osmium: 1% osmium tetroxide in 0.1M PHEM buffer

PHEM Buffer: 120 mM PIPES, 50mM HEPES, 4mM MgCl2.6H_2O, 20 mM EGTA in water, pH 7.4

Uranyl acetate: 1% uranyl acetate in distilled H_2O

II. Microwave procedure

1. Washes: 4x 40s PHEM Buffer;
2. 2x 7 min Osmium in PHEM (1:1) in vacuum;
3. Washes: 2x 40s PHEM Buffer;
4. Washes: 5x 40s water;
5. 7 min uracyl acetate in water (1:1) in vacuum;
6. Washes: 3x 40s water;
7. Dehydration:
    a. 40s 30% EtOH in water;
    b. 40s 50% EtOH in water;
    c. 40s 75% EtOH in water;
    d. 40s 90% EtOH in water;
    e. 3x 40s 100% EtOH;
8. Inflit:
    a. 3 min resin in EtOH (1:3) in vacuum;
    b. 3 min resin in EtOH (1:1) in vacuum;
    c. 3 min resin in EtOH (3:1) in vacuum;
    d. 3 min 100% resin in vacuum.

III. Lethalities

Table 6 – Mean lethality percentages obtained in each concentration. The lethality curves were performed with 5 or 6 concentrations of each drug. 3 or 4 replicates per condition were performed.

Gentamicin		**Paracetamol**	
Concentration (µM)	Lethality (%)	Concentration (µM)	Lethality (%)
419	2 ± 4,5	13231	0 ± 0,0
1256	60 ± 15,8	16538	2,5 ± 5,0
2094	84 ± 5,5	19846	10 ± 8,2
2931	94 ± 8,9	23154	62,5 ± 17,1
3769	96 ± 5,5	26462	87,5 ± 9,6
4188	98 ± 4,5	29769	100 ± 0,0

TFV		**TDF**	
Concentration (µM)	Lethality (%)	Concentration (µM)	Lethality (%)
8704	2 ± 4,5	1574	0 ± 0
10445	6 ± 8,9	2360	0 ± 0
12186	2 ± 4,5	3147	5 ± 5,8
13927	22 ± 26,8	3934	95 ± 5,8
15668	52 ± 17,9	4721	100 ± 0
17409	90 ± 14,1		

IV. Other techniques performed

a. Fluorescence Activated Cell Sorting (FACS)

50 to 60 *nacre wt1b::GFP; cdh17::GFP* larvae (4dpf) were exposed to the LC10 or LC10/10 of each drug for 24 hours. After drug exposition, larvae were placed in 15 mL falcon tubes and euthanized with ice. Then, EM was removed and 1 mL of HBSS w/ Mg^+ and Ca^+ plus 20 µL 10 mg/mL proteinase K and 50 µL 20 mg/mL collagenase were added. The larvae were incubated at 32ºC for 10 min and mechanical dissociation was applied every 5 min, by pipetting up and down. The mixture was centrifuged at 1200 g for 5 min and the pellet was resuspended in 1 mL of 5 mM EDTA. Mechanical dissociation was applied and the solution was centrifuged at 1200 g for 5 min. The pellet was resuspended in 1 mL of 0,25% trypsin, 1mM EDTA and incubated at 32ºC for 30 min. Mechanical dissociation was applied every 10 min. 10 mL of L-15 medium plus 1 mL of FBS was added to stop the digestion and the solution was incubated at 28ºC for 5 min. The mixture was centrifuged at 1200 g for 5 min and the pellet was ressuspended in 0,5 mL of L-15 medium. The cell suspension was filtered into flow cytometry tubes and a few drops of L-15 medium were added to clear the filter of remaining cells and thus maximize the cell retrieval. Cell suspension was centrifuged at 1200 g for 5 min and ~300 µL of supernatant was discarded. The pellet was ressuspended in the remaining liquid and analyzed in the FACSaria (Benchtop, Becton Dickinson) or MoFlo (Dako Cytomation, now owned by Beckman Coulter) high speed cells sorters. Non treated *casper* larvae were always used as negative controls for auto-fluorescence correction. After FACS, cells were captured in 200 µL of L-15 medium and stored in 50 µL of PBS at -20ºC.

b. DNA extraction

DNA of cells obtained through FACS was extracted with the DNeasy blood & tissue Kit (Quiagen), according to the fabricant instructions (Annex VII), and diluted in Elution Buffer. DNA was quantified by the Nanodrop (Thermo NanoDrop 2000) and adjusted to 4 ng/µL.

c. qPCR

Mitochondrial DNA (mtDNA) was quantified by Real Time PCR (qPCR) using the LightCycler® 96 System (Roche) and the FastStart Essential DNA Green Master Kit (Roche). Each qPCR reaction had a final volume of 10 µl, with 1.5 µL DNAse free water (Roche kit), 0.5 µL Fw primer (10 µM), 0.5 µL Rv primer (10 µM) (Table 6), 5 µL Master Mix (Roche kit) and 2.5 µL DNA sample (4 ng/µL) or water.

The thermal cycling protocol was as follows: initial denaturation for 10 min at 95ºC, followed by 45 cycles of 10s at 95ºC (denaturing), 10s at 60ºC (annealing) and 10s at 72ºC (extension). A melting curve was performed to confirm that only specific products were amplified. Primers against nuclearDNA were used in parallel with mtDNA to correct for variability, as the quantity of nuclearDNA is considered to be stable within cells. Data was obtained as relative quantification of mtDNA, through the calculation of mtDNA / nuclearDNA ratio. DNA samples with 2 ng/µL and 1 ng/µL were used as controls to confirm the maintenance of the mtDNA / nuclearDNA ratio.

Table 6 – mtDNA and nuclearDNA primers used for the qPCR.

	Forward (Fw)	Reverse (Rv)
Mitochondrial	5'-CAAACACAAGCCTCGCCTGTTTAC-3'	5'-CACTGACTTGATGGGGGAGACAGT-3'
Nuclear	5'-ATGGGCTGGGCGATAAAATTGG-3'	5'-ACATGTGCATGTCGCTCCCAAA-3'

V. qPCR procedure

1. Cells (between $4x10^6$ and $5x10^6$) were centrifuged for 5 min at 190 rpm in 200 µL PBS; supernatant was discarded;
2. 20 µL proteinase K plus 200 µL buffer AL were added and samples were thoroughly mixed by vortex and incubated at 56 °C for 10 min;
3. 200 µL ethanol (96-100%) were added and samples were mixed by vortex;
4. Mixture was pipetted into a DNeasy Mini spin column placed in a 2 mL collection tube and then centrifuged at 8000 rpm for 1 min; flow-through and collection tube were discarded;
5. The spin column was placed into a new 2 mL collection tube and 500 µL Buffer AW1 were added; spin columns were centrifuged at 8000 rpm for 1 min; flow-through and collection tube were discarded;
6. The spin column was placed into a new 2 mL collection tube and 500 µL Buffer AW2 were added; spin columns were centrifuged at 14000 rpm for 3 min; flow-through and collection tube were discarded;
7. Step 6 was repeated and then spin column was placed into a new 1.5 mL tube;
8. DNA was eluted by adding 50 µL and incubated for1 min at room temperature; spin column was centrifuged at 8000 rpm for 1 min;
9. DNA samples were stored at -20°C.